Koninklijk Nederlands
Meteorologisch Instituut
Ministerie van Infrastructuur en Milieu

Evaporation-Precipitation Coupling in a Global Climate Model (EC-earth)

Sem Vijverberg
Utrecht University

supervised by
Dr. Frank Selten (KNMI)
Dr. Aarnout van Delden (UU)
Dr. Ruud van der Ent (UU)

August 7, 2017

Contents

Abstract

State of the art climate models still render substantial present-day biases over land, most notably in summer, i.e. the mean of (most) global climate models render a strong underestimated of evaporation and precipitation in (semi-) dry regions, while overestimating these fluxes in the wet regions. These biases in the hydrology strongly affect the surface temperature biases in summer. In order to improve the surface biases of global climate models, an accurate hydrology is crucial. This study emphasizes the importance of the correct evaporation-precipitation coupling to achieve the correct hydrology (soil water content, evaporation, precipitation) in all seasons. Furthermore, the study elucidates the non-local impact of evaporation on precipitation.

In the first results section, we compare the hydrology of EC-earth versus the reanalysis ERA-Interim using a moisture tracking scheme. We implement a moisture tracking scheme to track all water from continental evaporation forward in time, which allowed us to analyse how precipitation and continental evaporation are linked. Our analysis indicates that the evaporation-precipitation coupling is stronger in EC-earth. Obviously, a too strong evaporation-precipitation coupling works in both ways. Thus, the precipitation response can feedback on an initial deficit or excess in evaporation. In the seasonal cycle context, this means that the precipitation response can amplify drying that is initiated in spring. In regions where evaporation is limited by the soil water content, precipitation will respond too strongly to the arising decrease in evaporation in (semi-) dry regions. Conversely, where continental evaporation is not limited by the soil water content, the evaporation will increase in spring and will lead to an overestimation of precipitation.

In the second part of this research, we examine EC-earth's response to a heterogeneous perturbation that increased the runoff in (semi-) dry regions. We find propagation of drought throughout summer, which is not directly forced by our perturbation. The direct impact of the increased runoff leads to drying, indirectly, the drying of the soil is affecting its surroundings, referred to as the quasi-local impact. Conclusively, the drier soils are further propagating drought indirectly through (1) the quasi-local impact of evaporation on precipitation and (2) the quasi-local decrease in clouds.

In the third part, we investigated the link between source and destination of atmospheric water. We show where most of the continentally evaporated water is accumulating in the atmosphere, i.e. the destination. By decreasing the continental evaporation, we observed a substantial decrease in the (remote) destinations of continental water. Thereby proving there is a clear connection between source and destination of water. The link between source and destination of precipitation was found less robust because the atmosphere is responding to a decrease in (continental) water content. Hence, the atmospheric responds generally increases the amount of water in the column from oceanic origin. The total amount of water in the atmosphere even increased in some regions. Conclusively, there is a link between source of water and precipitation, but it can be diminished (or even reversed) due to the increase in (oceanic water) convergence.

1 Introduction

Global Climate Models (GCMs) provide both future projections, and increased understanding of the climate system. The ability to simulate the climate system has improved over time (Reichler and Kim, 2008), however, current state of the art climate models still show systematic regional biases over land when simulating present day climate (Mueller and Seneviratne, 2014). Focussing on the northern hemisphere summer, dry regions are generally associated with substantial underestimation of both evaporation and precipitation, see figure 2. Conversely, wet regions generally overestimate evaporation and precipitation. Reducing the present day biases is important for the ability of climate model to make future projections (Boberg and Christensen, 2012; Sippel et al., 2017). An unpublished study, referred to as the SRO-experiment, within the Royal Netherlands Meteorological Institute demonstrates the impact of a moderate increase in surface-runoff (SRO) on the climate change signal, and the present-day climate (see Fig. 3). Among other results, the study shows a decrease in precipitation and warmer summer surface-temperatures up to 3.5°. Even the climate change signal is enhanced due to the moderate increase in surface-runoff, depicting the sensitive interaction between land surface hydrology and atmospheric surface conditions. Moreover, output of global climate models is often used for downscaling (Feser et al., 2011), thereby, regional biases of the global climate models are passed into the regional domain via the boundary conditions.

In order to improve these regional biases, an accurate soil moisture content is essential (Seneviratne et al., 2013; Lorenz et al., 2016; Haarsma et al., 2009; Seneviratne et al., 2010). Soil-moisture directly affects land-atmosphere fluxes of energy and water mass; mainly by altering the partitioning of net incoming radiation into sensible, latent and ground heat fluxes and to smaller extent by changing the albedo of the soil. Indirectly, soil moisture interacts with the vegetation abundance and/or condition, potentially altering the transpiration (as noted by Fischer et al. (2007); Mintz (1982)) and albedo of the plants (Teuling and Seneviratne, 2008). In this report, we address special attention to the link between evaporation and precipitation, see section 2.1 for a detailed description of the evaporation-precipitation interaction.

In a GCM, the land surface-scheme regulates the fluxes and evolution of the soil water content (see schematic figure 1a). It is important to realize that the impact of soil desiccation is the end result of numerous interactions between the soil and atmosphere, which are all mediated via evaporation (see method section 2.1). To keep the soil water volume, and thus evaporation, accurate throughout the year, the correct correct response of precipitation to a change in evaporation is imperative (Taylor et al., 2012). Hohenegger et al. (2009); Taylor et al. (2013) showed there are substantial differences in the precipitation response to a soil-moisture anomaly depending on the convective scheme. Unfortunately, quantifying the coupling strength is very difficult (Lintner and Neelin, 2009). However, the evolution of soil water content throughout the year is likely affected by the evaporation-precipitation coupling strength Taylor et al. (2012).

Despite the apparent importance, the link between evaporation-precipitation coupling strength has received little attention. It remains unsettled to what extent the evaporation-precipitation coupling affects surface conditions. Another caveat is that the impact of a decrease in evaporation on precipitation is generally studied locally, with the exemption of Zampieri et al. (2009). Considering our global climate models exhibit a substantial underestimation of evaporation in the dry regions of the world, how does this anomaly affect its surroundings? To specify, to what extent is evaporation affecting precipitation non-locally? This study aims to shed a new light on the link between evaporation and precipitation.

This research can be subdivided into two parts. In preliminary research (also presented in this report), we evaluate the source of moisture which precipitated in central Europe in the global climate model EC-earth. Subsequently quantifying the accuracy of the source by benchmarking it against the ERA-Interim reanalysis dataset. We also compare where the evaporation from our central European region will precipitate. These first results show that EC-earth is simulating a higher amount of recycled moisture. The increase in moisture recycling is, among other things, affected by the coupling strength between continental evaporation and precipitation.

Successively, we start to evaluate the importance of evaporation for precipitation on a continental scale. We investigate if EC-earth is simulating a stronger continental evaporation-precipitation coupling and elaborate on the consequence of a stronger coupling on the soil water content. The 'evaporation-precipitation coupling analysis' is backed by a moisture tracking scheme (see method section 2.3).

In the second part, we investigate the impact of a change in the surface-runoff description (the SRO-experiment mentioned above) in further detail. Only (semi-) dry regions are affected by our increased surface-runoff. This allows us to observe how the perturbation is affecting its surroundings. Additionally, we investigate if there is a remote link between the source and destination of atmospheric water. The change in atmospheric water content can mediate changes in precipitation. With the moisture tracking scheme, we are able to separate water from continental or oceanic origin. Since our perturbation only lowers the continental evaporation, we can evaluate how this affects continental water storage in the atmosphere.

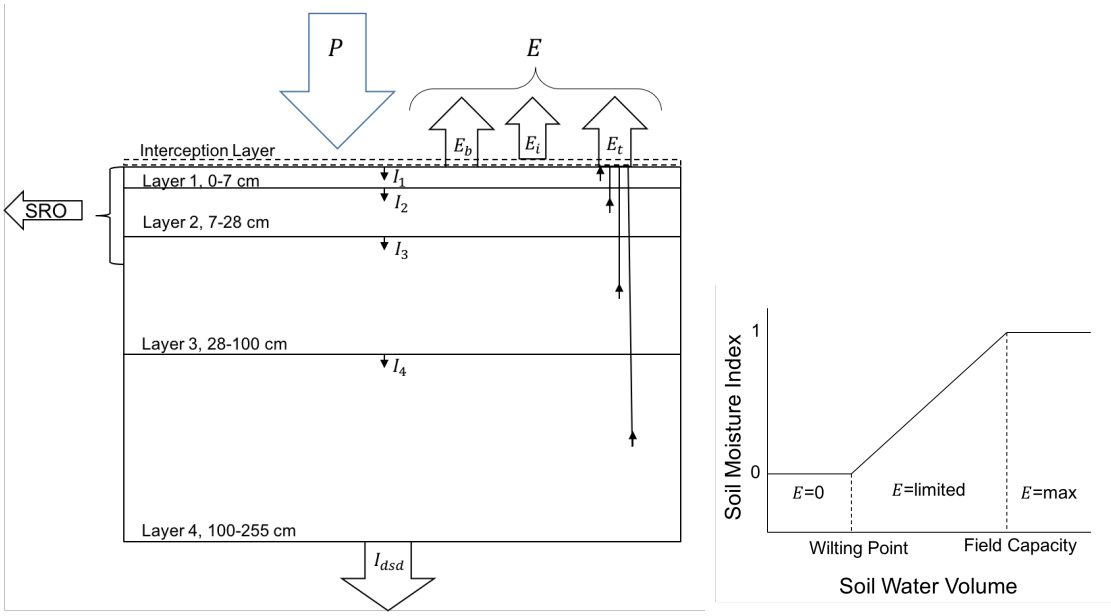

(a) (b)

Figure 1: (a) Simplified Schematic representation of the land surface-scheme (H-TESSEL) used in EC-earth. I_L represents the infiltration of each layer, SRO represents surface-runoff, I_{dsd} represents deep soil drainage. E_b, E_i and E_t stand for evaporation of soil water, intercepted water and transpired water. In this report, the term evaporation (E) refers to the sum of all E_b, E_i and E_t fluxes and runoff (R) refers to SRO+I_{dsd}. (b) Relation between soil water volume (θ) and evaporation, showing the impact of the wilting point (θ_{wp}) and field capacity (θ_{fc}). Based on the link between soil water content and evaporation, different soil moisture regimes can be discriminated (Seneviratne et al., 2010). When $\theta \leq \theta_{wp}$, all evaporation is ceased, when $\theta \geq \theta_{fc}$, evaporation is no longer restricted by soil water content, only by radiative energy. Between wilting point and field capacity evaporation is limited by both the soil water content and energy. In this report, we discriminate between moisture-limited soil regimes ($\theta \leq \theta_{fc}$) and energy-limited soil regimes ($\theta \geq \theta_{fc}$).

2 Method

2.1 Soil Moisture-Precipitation Interactions

Evaporation-Precipitation interactions and soil moisture-precipitation interaction are principally identical, although the latter takes into account the link between soil moisture and evaporation, visualized in figure 1b. When the soil water volume (θ) is below the field capacity (θ_{fc}), evaporation is limited, in this report referred to as a moisture limited regime. When the soil water volume (θ) is above the field capacity (θ_{FC}), the evaporation is only limited by the amount of radiative energy available, hence, referred to as a energy-limited soil regime.

The *direct* effects of soil moisture - described in the first paragraph of the introduction - can influence precipitation in 3 different ways; (1) by altering the stability of the boundary layer (Santanello et al., 2009) (2) by altering the atmospheric moisture content, and (3) soil moisture anomalies can affect atmospheric circulation (Fischer et al., 2007), inducing associated precipitation changes. These 3 mechanism will be elucidated later in this text. We separate the evaporation-precipitation interaction, following the nomenclature similar to Goessling and Reick (2011) (with a slight adjustment in the naming and definition of mechanism 2).

(1) The impact on the stability of the boundary layer is referred to as local evaporation-precipitation coupling, or local coupling. The local coupling can be positive or negative. Two opposite coupling mechanisms are described by (Hohenegger et al., 2009). Firstly, a positive soil moisture anomaly can increase the moisture content of the planetary boundary layer (PBL) by increasing evaporation and lowering the PBL-height due to a lower sensible heat flux (weaker convection due lower vertical temperature gradient). This leads to an increase of the moist static energy and increases the potential for convective development, i.e. favouring conditions for precipitation over wet soils. Conversely, convection can also be triggered by a negative soil moisture anomaly, which is able to increase the PBL-height up to the level of free convection.

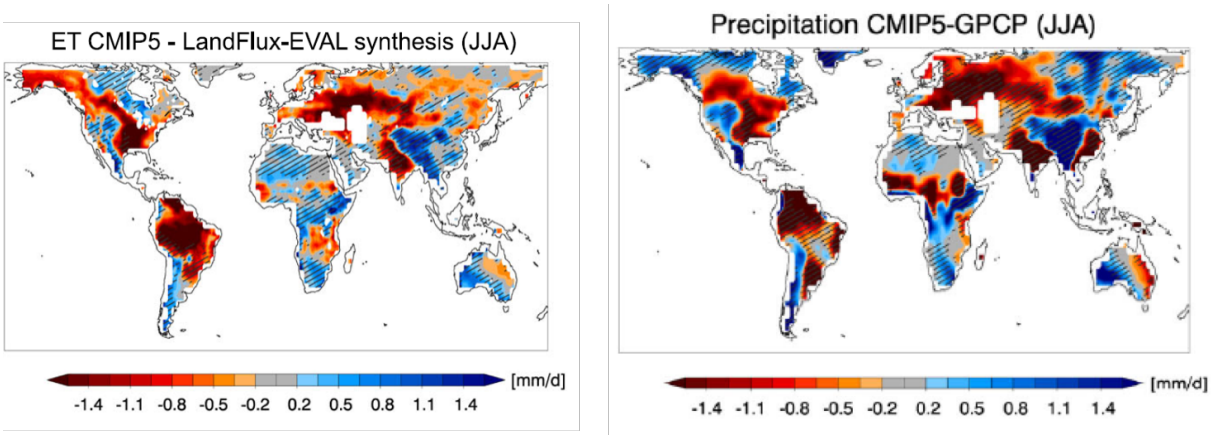

Figure 2: CMIP5 June to August mean versus reference datasets of evaporation and precipitation. The reference product for evaporation (ET) is the LandFLux-EVAL merged synthesis product, for precipitation the GPCP data set. The stripes indicate where 10 out of 14 CMIP5 models agree on the sign of the differences.

(2) The 'water mass recycling' precipitation changes due to a change in the total atmospheric water content, i.e. precipitable water.

(3) The soil moisture available for evaporation on land plays an important role for large scale circulation. Therefore, teleconnected precipitation changes can occur due to changes in circulation. Mintz (1982) performed an illustrating experiment in which he forced all land to be moist and fully covered with vegetation. The surface pressure over land increased, and for the Northern summer, the land-sea surface pressure contrast largely vanished. Kleidon and Heimann (2000) looked at the impact of allowing deeper roots in global climate models (GCM's), instead of the often prescribed 2 meter rooting depth. Due to increased rooting depth, he found an intensification of the tropical (Hadley) circulation patterns.

Note, these mechanism are only describing the direct effects. To capture the full soil moisture-precipitation interaction, clouds play a particularly important role. Changes associated with the mechanisms described above - water content, stability and circulation - can all affect the formation of clouds. Via altering the surface shortwave and longwave radiation, clouds affect the amount of radiative energy available at the surface. Generally, a decrease in clouds renders an increase in the available radiative energy (with the exemption of very high albedo surfaces). Consequently, evaporation will increase, thereby, the cloud response will feedback on mechanism described above.

2.2 Moisture Recycling

Moisture recycling has sometimes been interpreted to be a measure of how much of the local precipitation is *due to* the local evaporation, but this is inaccurate. For example, if the triggering of precipitation occurred due to e.g. moisture convergence, a part of the water in the column with local origin will precipitate locally and, hence, be allocated to recycled moisture (while this precipitation could have occurred without any contribution of local evaporation). Moisture recycling quantifies the local precipitation that stems from local evaporation. The amount of locally recycled moisture is to a large extent governed by the potential of local evaporation to accumulate in the atmospheric column aloft its local domain. Hence, a stronger moisture flux will lower the moisture recycling, since it reduces the accumulation (due to quicker advection of the locally evaporated water out of the domain). A higher evaporation will enhance the moisture recycling, since the source flux into the atmosphere is higher.

Investigating moisture recycling is regularly done numerically, by implementing a moisture tracking scheme (see Goessling and Reick (2011) and references therein). By tracking the evaporated water from a certain region in time (Eulerian, e.g. Van Der Ent et al. (2013) or Lagrangian e.g. Dirmeyer and Brubaker (2007)), one can find where this water will precipitate. If this water rains out within the same region, it can be referred to as regionally recycled moisture. With this information, the regional precipitation recycling ratio (ρ_r) is defined as,

$$\rho(t,x,y|A,\zeta)_r = \frac{P_r(t,x,y|A,\zeta)}{P_r(t,x,y|A,\zeta) + P_a(t,x,y|A,\zeta)} = \frac{P_r(t,x,y|A,\zeta)}{P(t,x,y|A,\zeta)}, \tag{1}$$

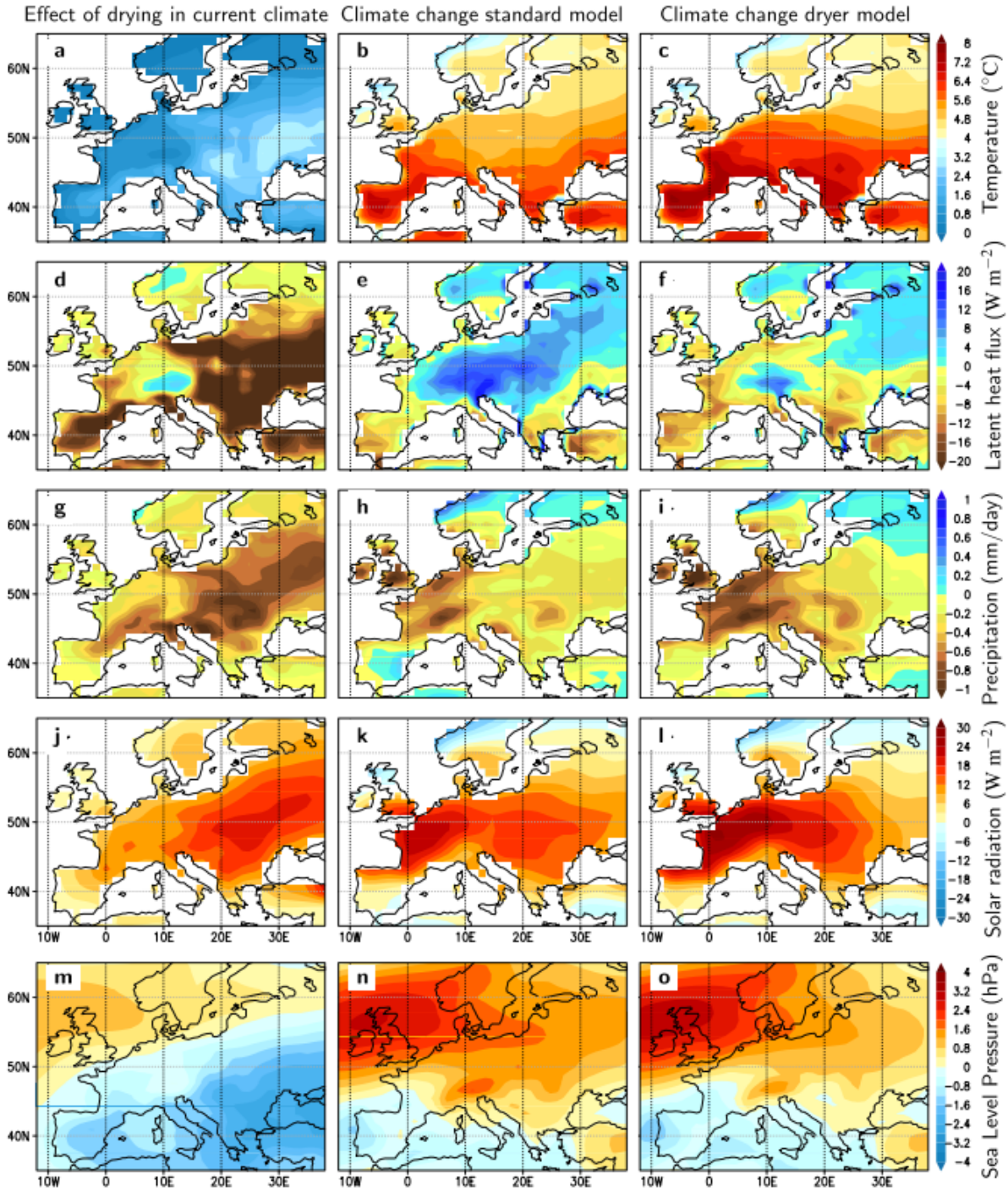

Figure 3: The SRO-experiment results. The first column shows the differences in the current climate (1981-2010) between the simulation with a more efficient surface runoff (see section 2.5.1) and the control simulation using EC-earth. The second and third depict the climate change between 2071-2100 and 1981-2010 for the control simulation and the more efficient surface-runoff simulation, respectively. Panels (a-c) show surface air temperature (°), (d-f) surface evaporation expressed as the surface latent heat flux (W m^{-2}), (g-i) total precipitation (mm day^{-1}), (j-l) net surface solar radiation (W m^{-2}) and (m-o) mean sea-level pressure (hPa).

where, P_r is the recycled precipitation, and P_a is the precipitation of moisture that was advected into the region and P is the total precipitation. Similarly, the evaporation recycling ratio (ϵ_r) is defined as,

$$\epsilon(t,x,y|A,\zeta)_r = \frac{E_r(t,x,y|A,\zeta)}{E_r(t,x,y|A,\zeta) + E_a(t,x,y|A,\zeta)} = \frac{E_r(t,x,y|A,\zeta)}{E(t,x,y|A,\zeta)}, \tag{2}$$

where, E_r is the evaporation which originated from the region and will be replenished by precipitation, i.e. recycled evaporation, and E_a is the part of evaporation from the region that is advected out of the region and E is the total evaporation.

Note, regional recycling ratios are also dependent on the surface area (A) and shape (ζ) of the region, since a large (rectangular) region (parallel to the moisture flux) will have a higher recycling ratio compared to a small region (perpendicular to the moisture flux). Other metrics were developed to allow comparisons between moisture recycling studies (Van Der Ent and Savenije, 2011; Goessling and Reick, 2011; Van Der Ent et al., 2010). One solution is to track all the continents (Van Der Ent et al., 2010), since continents are (to good approximation) the same in all models, hence, comparable. This analysis leads to the definition of the continental precipitation recycling ratio (ρ_c),

$$\rho_c(t,x,y) = \frac{P_c(t,x,y)}{P_c(t,x,y) + P_o(t,x,y)} = \frac{P_c(t,x,y)}{P(t,x,y)}, \tag{3}$$

where, P_c (and P_o) is precipitation, which stems from continental (oceanic) evaporation.

2.3 Moisture Tracking Scheme

The tracking of moisture allows us to visualize the destination of evaporation (forward tracking) and source of precipitation (backward tracking) from a chosen region. The tracking is done for two datasets: ERA-Interim and a single member of EC-earth v2.3 (see appendix 'model specifications' for details). The models are comparable, yet the most important difference between the two models is that the physics of EC-earth is allowed to run free, while ERA-Interim fields are constrained by observations every 6 hrs (Dee et al., 2011).

The tracking is done with the (Eulerian-based) Water Accounting Model-2layers (WAM-2layers) developed by Rudi van der Ent (van der Ent, 2014, 2016). The 'core of the model' requires the water content and horizontal moisture fluxes of each grid point on approximately 20 vertical levels. The 20 vertical levels are subsequently downscaled to two layers, in order to account for potential wind shear, with the interface at approximately 850 hpa. First, the full global atmospheric hydrology is calculated for the two vertical layers using the information from the input model of the water content, evaporation, precipitation and moisture fluxes. The vertical moisture flux is calculated by using the water mass balance,

$$\frac{\partial S_k}{\partial t} = \nabla(S_k\vec{v}) + E_k - P_k \pm F_v + \epsilon_k \qquad [\mathrm{L}^3\mathrm{T}^{-1}], \tag{4}$$

where S_k is the moisture storage in layer k, t is time, $\nabla(S_k\vec{v})$ is the moisture convergence flux, E_k is evaporation, P_k is precipitation, F_v is the vertical moisture flux and ϵ_k is a small error that is made due to coarser vertical and temporal resolution of WAM with respect to the full model. The vertical water flux F_v is calculated based on the water content field after the 't+1' numerical integration timestep within WAM-2layers, taking into account horizontal moisture convergence, evaporation and precipitation only. After this timestep, a mismatch will be present with respect to the water content in the full model at timestep 't+1'. The vertical flux is calculated based on this mismatch with the full model. In the model, evaporation is only added to the lower layer and precipitation is subtracted with weights corresponding to the water content of each layer. After this first procedure, a time series of the moisture field and horizontal and vertical fluxes is available in accordance with the full model (on the native model horizontal grid with two vertical layers).

When the model performs tracking forward in time, it uses the calculated moisture flux deduced from the input model as explained above. Hence, when evaporation from a tracked region enters the gridcell it will be transported with the pertinent moisture flux. The tracked evaporation will rain out following the well-mixed assumption; the amount will be proportional to the relative amount of water vapour in the gridcell (q_{tracked}/q):

$$P_{\mathrm{tracked}} = \frac{q_{\mathrm{tracked}}}{q} P \tag{5}$$

where, $q_{tracked}$ and q present the tracked and total water in the atmosphere, respectively. Similarly, $P_{tracked}$ is the precipitation of water that originating from the tracked region and P represents the total precipitation. This same procedure can also be done backward in time.

2.4 Moisture Tracking: EC-earth v2.3 vs. ERA-Interim

2.4.1 Evaporation and Precipitation fields

Within the climate community, it is generally known that the reputation of reanalysis datasets for being 'our best estimate of the climate' holds for state variables such as wind, temperature, pressure, and humidity, but that the calculated fluxes (radiation, heat fluxes, precipitation, evaporation) are prone to larger uncertainties since these variables are not constrained by observations (Dee et al., 2011; Trenberth et al., 2011). Therefore, we also test the accuracy of ERA-Interim by comparing monthly mean evaporation and precipitation field with observation(-based) datasets, see section 2.4.1. For precipitation, we use the Global Precipitation Climatology Project (GPCP) version 2.3 [1] and evaporation fields with the Global Land Evaporation Amsterdam Model (GLEAM) version 3. GPCP is a global (2.5° by 2.5°), monthly analysis (1979 - present) of precipitation Adler et al. (2003). It merges precipitation estimates from satellite microwave and infra-red data, and surface rain gauge observations and is accompanied by an error estimate. These gauge data are then used to constrain (and validate) satellite estimates, since rain gauge data over oceans is very scare, the associated error is larger. The error estimate encompasses only the random error due to algorithm and sampling errors. GLEAM uses a set of algorithms, which translates observations of soil moisture, vegetation, snow, air temperature, radiation and precipitation to find the terrestrial evaporation and root-zone soil moisture Martens et al. (2016). The observations rely on a large multitude of (merged) satellite based products, sometimes in combination with reanalysis products.

2.4.2 Moisture Tracking Central-Europe

To investigate the accuracy of the atmospheric moisture transport in EC-earth v2.3 we implement a moisture tracking scheme and benchmark it against the ERA-Interim reanalysis dataset. The differences are quantified by comparing the multi-year mean (from 1979 to 2014, 34 years) fields. The moisture tracking scheme requires input of multiple (3-dimensional) variables on sub-daily temporal resolution.

The first year of tracking in time is excluded from calculating the multi-year mean fields, since the tracked moisture storage fields will be empty at the start. In our first analysis, we select an identical region in central Europe in both models (referred to as the CEU-region) and track both the source of precipitation backward in time and the destination of evaporation forward in time. Subsequently, we investigate the difference in climatological source of precipitation and destination of evaporation between EC-earth and ERA-Interim. All the evaporated water from the CEU-region will be added to the tracked water in the atmosphere and will be labelled as tracked water (q_{tracked}). In the analysis, we restrict ourselves to the summer months June - August, since then the result of evaporation-precipitation interactions emerges most strongly.

2.4.3 Evaporation-Precipitation Coupling Analysis

To document the regional (CEU) differences in a broader spatial scale perspective, we analyse the differences in across the Eurasian continent. We expand our analyses in order to evaluate the coupling strength between evaporation and precipitation.

Firstly, we interpret differences in the climatological evaporation and precipitation fields. Secondly, we analyse the amount of precipitation originating from continental origin, referred to as the continental precipitation. If more precipitation is originating from continental origin, then the continental evaporation is playing a more important role. The amount of moisture recycling will be influenced by the (local) coupling strength between evaporation and precipitation. If this (local) coupling is strong, precipitation is more likely to be triggered nearby a positive evaporation anomaly. This causes the amount of recycled precipitation to increase, thus, it increases the continental precipitation recycling ratio. The amount of continental precipitation is also influenced by the amount of continental evaporation, therefore, we also need to consider the information from the difference in evaporation fields. Thirdly, we introduce a new land-precipitation metric (ζ). It is backed by information on both the atmospheric water composition q_c/q - where q_c denotes the water content from continental origin and q refers to the total column water - and the continental precipitation recycling ratio.

The zero-hypothesis of this metric is that precipitation has no preference for the atmospheric water content composition. When precipitation is more often occurring with above average amount of continental water in the total water column, then apparently, there is a link between continental evaporation and precipitation. In other words, that will indicate a stronger coupling between continental water and precipitation. The metric works as follows:

[1] GPCP Precipitation data provided by the NOAA/OAR/ESRL PSD, Boulder, Colorado, USA, from their Website at http://www.esrl.noaa.gov/psd/

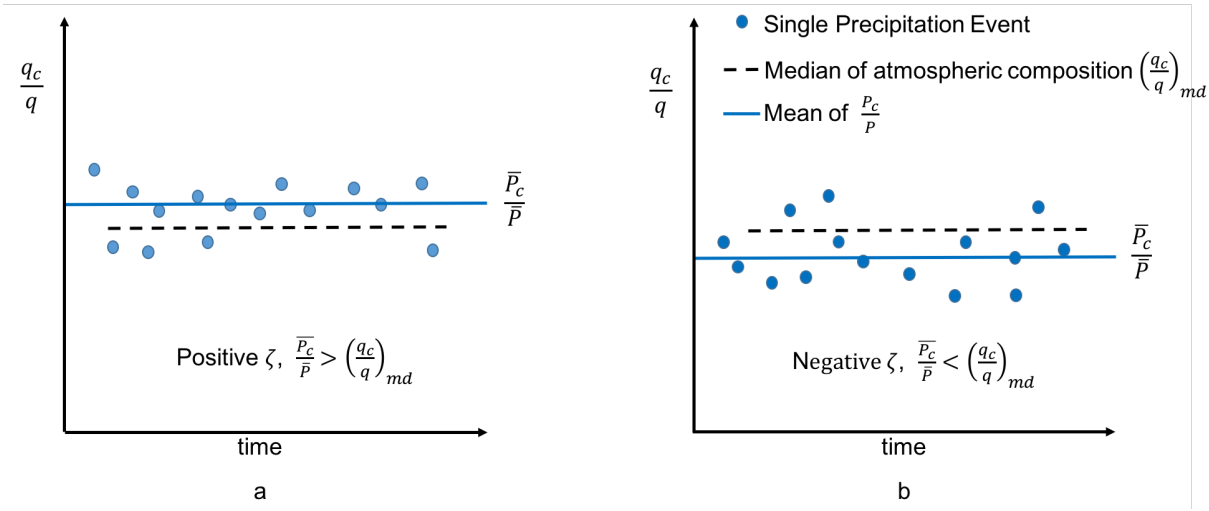

Figure 4: Land-precipitation metric ζ, where the zero-hypothesis is that precipitation has no preference for the atmospheric water content composition. If ζ is positive (a): precipitation is more likely to occur when continental water content is above the median (high q_c/q). If *zeta* is negative (b): precipitation is more likely to occur when oceanic water content is above the median (low q_c/q).

The climatological continental precipitation recycling ratio - as calculated by the moisture tracking scheme - depends on the climatological background composition of the water (the median of the water ratio, q_c/q). The continental precipitation recycling ratio will exceed the background state when precipitation events are more often co-occurring with a high $q_c(t)/q(t)$. Hence, calculating the difference in the ratio's;

$$\zeta = \frac{\bar{P}_c}{\bar{P}} - \left(\frac{q_c}{q}\right)_{\text{md}}, \tag{6}$$

renders a metric that will be (more) positive if precipitation events occur more often with high contribution of continental evaporation to the water content, see figure 4 for a visual representation. The $(\bar{})$ denotes the climatological time average. The land-precipitation metric is further evaluated in the CTRL-run of EC-earth, see appendix E.

Note, in the second part of the analysis we will interpret an absolute difference in continental precipitation recycling ratio, which is a non-trivial matter. Firstly because, the ratio ρ_c follows an asymptotic exponential over land from 0 to a maximum of 1 downwind. Mathematically, small ratio's are more sensitive to a (absolute) non-significant change in P_c. To avoid distraction by the small unimportant changes, the relative change in only plotted when the CTRL-value is above 0.3. The absolute difference in precipitation recycling ratio (due to a difference in recycling strength) will depend on the initial value (of the CTRL), see appendix for a sensitivity test. The land-precipitation metric relies on the same information, therefore, the conclusions on the difference in continental precipitation recycling ratio and land-precipitation metric will be of a more qualitative nature.

Since we do not posses sufficient samples of climatological mean to deduce its uncertainty, we use statistical information of the inter-annual variability (σ_{iav}) to estimate the standard deviation of the climatological mean, σ_{cm},

$$\sigma_{cm} = \frac{1}{\sqrt{N}}\sigma_{iav} = \frac{1}{\sqrt{N}}\sqrt{\frac{1}{N}\sum_{i=n}^{N}(y_n - \bar{y})^2}, \tag{7}$$

where N equals the number of years, y_n the value of variable y in year n, $\bar{y}$ the climatological mean. When the difference ($\Delta y[\text{lon}, \text{lat}]$) exceeds the 95% distribution ($2\sigma_{cm}$) of ERA-Interim, the (lat,lon) coordinate is hatched using dots (unless stated otherwise).

2.5 Surface-runoff (Sensitivity) Experiment

2.5.1 The surface-runoff Perturbation

A control run (CTRL) will be compared to a simulation with more efficient surface-runoff parametrization, referred to as (DRY). In the CTRL-run, the surface-runoff is given by,

$$\text{SRO} = T + M - I_{max}, \tag{8}$$

where, SRO is the surface-runoff, T is the throughfall precipitation (precipitation - intercepted water), M is the snow-melt and I_{max} is the maximum infiltration rate (i.e. vertical water flux) of water into the soil. Where surface-runoff depends on the standard deviation of the surface orography and the saturated (W_{sat}) and actual (W) water content integrated over the first 50 cm of soil, defined as an effective depth for surface-runoff (Balsamo et al., 2009). The saturated water content (W_{sat}) is the maximum water holding capacity of the soil, hence, dependent on soil hydraulic diffusivity and conductivity. When the soil water content (W) in the top layer is greater than the corresponding saturated water content (W_{sat}), the excess will be attributed to surface-runoff. Whenever throughfall or snowmelt occurs, the inflow will be partitioned between surface-runoff and infiltration (Balsamo et al., 2009). In our (DRY-run) experiment, the surface-runoff (SRO) is described by,

$$\text{SRO} = \begin{cases} T + M - I_{\max} & \text{if SRO}/P > 20\% \text{ of P} \\ 20\% \text{ of P} & \text{if SRO}/P < 20\% \text{ of P} \end{cases}$$

where P is precipitation. Hence, surface-runoff is now always at least 20% of the precipitation. Note, the sum of 'surface-runoff' and 'deep soil drainage' together comprise the 'runoff', i.e. the cumulative land water sink excluding evaporation. In this work, evaporation encompasses all transport of water from the soil to the atmosphere, i.e. bare soil evaporation, and evaporation of transpired or intercepted water, see schematic representation of the land surface scheme in figure 1.

2.5.2 Analysis

The impact of increased runoff in summer and spring are discussed in more detail in the appendices C and D, respectively. Our main storyline conveys the non-local impact of evaporation on precipitation. With the new surface-runoff (SRO) formulation, only regions where the native-formulation of SRO is below 20% of the precipitation (P) will be raised to 20% of P (see section 2.5.1). Unfortunately, the experiment did not store surface-runoff and 'deep soil drainage' separately. Therefore, we present the efficiency of the runoff sink (R = SRO + deep soil drainage) with respect to the precipitation. The efficiency of SRO will be lower, however, (monthly mean) deep soil drainage and surface-runoff are closely coupled. Advantageously, it directly captures the sink via land surface gridcell-to-gridcell water exchange. By comparing the DRY versus CTRL-run, we visualize how the new surface-runoff formulation affects runoff and the soil water content (section 4).

Section 4.1 concentrates on the precipitation response at the peripheries of an evaporation anomaly, i.e. the quasi-local impact of evaporation on precipitation. The large impact of the wilting point on evaporation is addressed separately in section 4.2. Our last section emphasizes the remote impact of evaporation on precipitation. We implement the moisture tracking scheme to track all continental water in the atmosphere, and subsequently, we can visualize where continental water is accumulating in the atmosphere, i.e. the destination of continental water. If there is a link between source and destination of continental water, we expect a (remote) decrease in these 'destinations of continental water' when we decrease continental evaporation. Successively, we discuss how the change in continental water content is affecting precipitation.

As done previously, the differences in the climatological mean value of variables of interest are presented (from 1965 to 2003, 38 years). The significance is calculated as presented in section 2.4.3, the difference (DRY-CTRL) is hatched with dots when it exceeds $2\sigma_{cm}$ of the CTRL.

3 Results: Hydrological Performance EC-earth

3.1 Evaporation and Precipitation fields

To obtain insight in the accuracy of the evaporation and precipitation fields, we plot the latter of ERA-Interim and EC-earth and compare them to observation(-based) datasets as discussed in the method section. If we demarcate ourselves to the region that we will track, the precipitation bias with respect to GPCP is of larger magnitude in ERA-I (spatial mean of -0.40 mm/day) compared to EC-earth (+0.26 mm/day). For entire Eurasia, the absolute evaporation bias of both models are approximately equal with respect to the GLEAM dataset. However, ERA-Interim overestimates the evaporation in dry regions (lower Eurasia), while EC-earth renders an underestimation. The global evaporation and precipitation fields from both GLEAM and GPCP are presented in appendix B to provide context for the presented biases in figure 5 and 6.

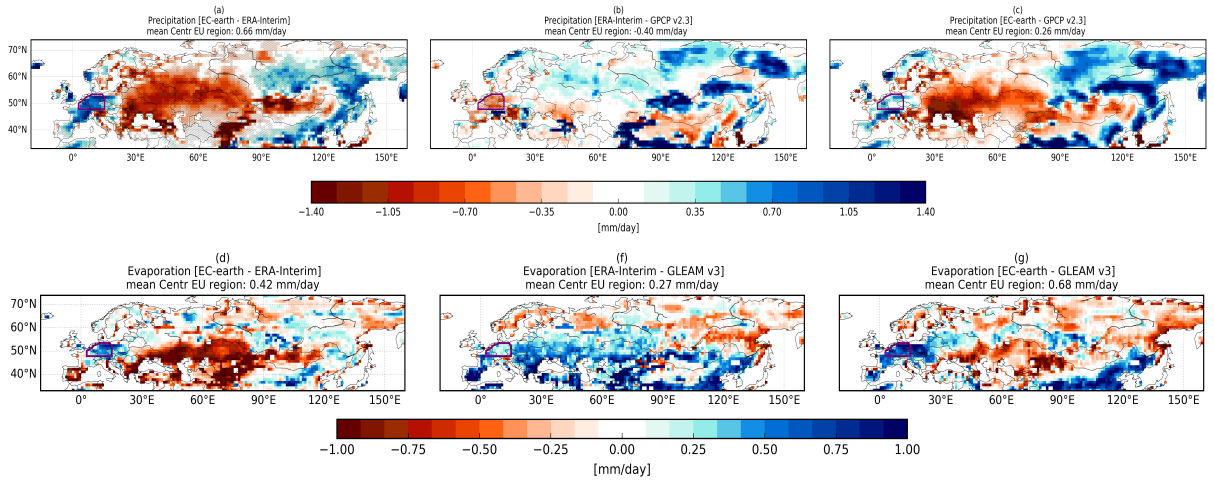

Figure 5: Difference in mean precipitation (a-c) and evaporation (d-f) fields for JJA (1980-2010) between ERA-Interim, EC-earth and the GPCP v2.3 dataset. The hatching in plot (a) signifies that the difference is larger then the 95% range of values in the ensemble spread by EC-earth' based on 8 members. (d-f) Difference in mean evaporation fields (1980-2010) between ERA-Interim, EC-earth and the GLEAM dataset. For the precipitation field, the GPCP v2.3 is accompanied by a random error estimate, thus exclusive of the systematic error. If the precipitation bias between the (reanalysis-)model and GPCP falls outside the 95% error range, the gridcell is hatched. However, the error is almost everywhere higher then the signal. When evaluating the precipitation difference between EC-earth and ERA-Interim, the hatching depicts where the signal is significant with respect to EC-earth' inter-ensemble spread of the climatological precipitation field.

3.2 Moisture Tracking

Figure 7 shows the result of backward tracking of precipitation for ERA-Interim, EC-earth and their difference (column 1, 2 and 3, respectively). The tracked region is depicted by the enclosing purple line and referred to as CEU-region. Figure 7a, b are showing the spatial distribution of the evaporative source strength (E_{tr}) for precipitation in the CEU-region (P_{region}), in both absolute terms (upper colorbar, mm/day) and the associated relative contribution to the total precipitation (bottom colorbar, % of E_{tr}). The latter percentage is a cumulative value, e.g. on the bottom colorbar the (*second*) darkest color blue represents a source strength stronger then (*0.15*) 0.3 mm/day, which is accountable for (*12*) 1% of the total precipitation in the region in ERA-Interim. This type of plot is referred to as an evaporation-shed, see Keys et al. (2014) for more information. The lower limit of the colorplot is arbitrary, yet equal for both models and thus comparable. The vectors depict the vertically integrated moisture transport. The figures 7a and 7b show that the evaporative source pattern is quite similar. Albeit, we observe that EC-earth has a stronger regional source strength (see figure 7c and the second colorbar percentages).

Figure 7a-c show the source strength relative to the total evaporation, i.e. it represents the ratio of evaporation that will precipitate in region-CEU. Similarly, we observe that the evaporative sources close to, or within the region

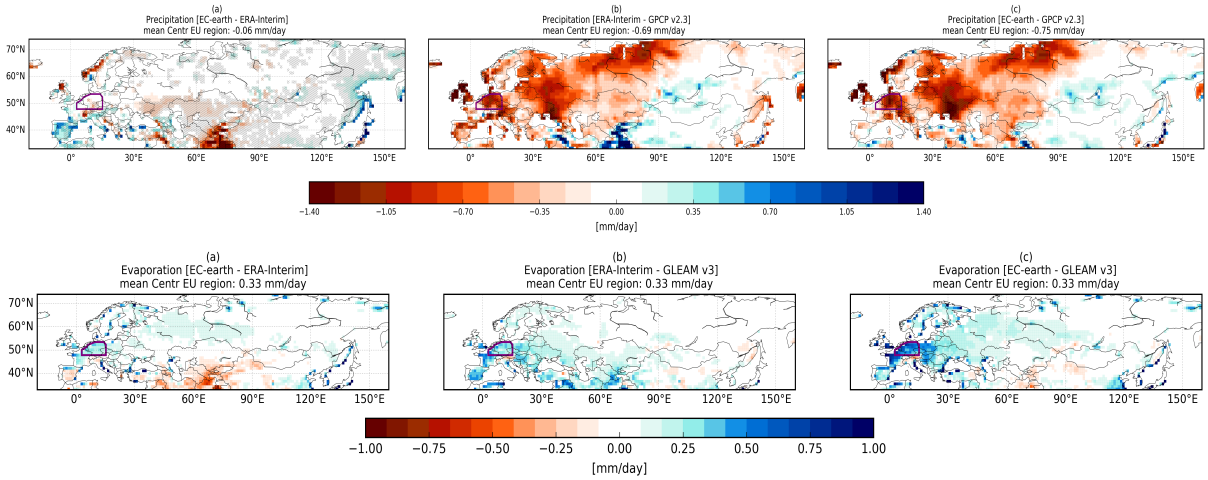

Figure 6: Difference in mean precipitation (a-c) and evaporation (d-f) fields for DJF (1980-2010) between ERA-Interim, EC-earth and the GPCP v2.3 dataset. See caption figure 5 for information.

are more dominant in EC-earth. Within region-CEU, the colors represent the regional evaporation recycling ratio. On average 11% of the evaporation will precipitate within the region in EC-earth, compared to 7% in ERA-Interim.

The tracked precipitation (P_{tr}) is shown in figure 8, i.e. the result of forward tracking of the evaporation originating from the CEU-region. Similar to our previous result, the evaporation originating from the region leads to a stronger precipitation close to or within the region both in absolute as in normalized terms, see figure 8a-c and 8 d-f, respectively.

We acknowledge that ERA-Interim does not show sufficient consistency with observations to discriminate the absolute bias found between EC-earth and ERA-Interim in the tracking, see figure 7c. The moisture recycling ratio's are not affected by the absolute biases since it display a ratio (tracked/total). The plots in figures 7d and 8e convey that a higher portion of the precipitation in (and close to) region-CEU stems from within (and close to) the region-CEU. Based on our small CEU-region and considering the substantial regional evaporation and precipitation biases found in ERA-Interim, we argue that the result is insufficiently *accurate* to state that EC-earth is overestimating the moisture recycling with respect to reality.

However, we observe a more robust signal when considering the entire Eurasian continent in JJA, i.e. precipitation in ERA-Interim is similar to the observed GPCP dataset while EC-earth's bias is large. It is proven (and expected) that the amount of continentally recycled moisture significantly increases during the spring/summer season (Van Der Ent et al., 2010). Coincidentally, we observe a change in the magnitude and spatial pattern of the precipitation- and evaporation bias (transition of figure 6 towards figure 5). The increase in bias can obviously have numerous causes, such as the deficiencies in the land-surface scheme and parametrization of (moist) convection, precipitation and clouds.

Hereafter, we focus on the importance of the coupling strength between evaporation and precipitation. The increased precipitation recycling that was found in central-Europe, can be the result of a stronger link between local evaporation and local precipitation. We suspect that the biases in evaporation and precipitation are partly caused by an overestimation in the evaporation-precipitation coupling. Therefore, in the following section, we asses the continental precipitation recycling ratio, the land-precipitation metric and take into account the biases found in evaporation and precipitation, in order to evaluate the coupling strength on a continental scale.

3.3 Evaporation-Precipitation Coupling Strength: EC-earth vs. ERA-Interim

To evaluate the relation between the large hydrological biases and recycling in summer, we plot the absolute (EC−ERA) and relative differences ((EC−ERA)/ERA) in the evaporation and precipitation fields over Eurasia, see figure 10. Figure 11a, b show the continental precipitation recycling ratio of ERA-I and the difference (EC-ERA) for summer, respectively.

The continental precipitation recycling ratio is much higher in summer compared to winter (Fig. 12a), since in summer there is simply much more continental evaporation contributing to the atmospheric water. We show that EC-earth's continental precipitation recycling is higher inland compared to ERA-I both in summer and in

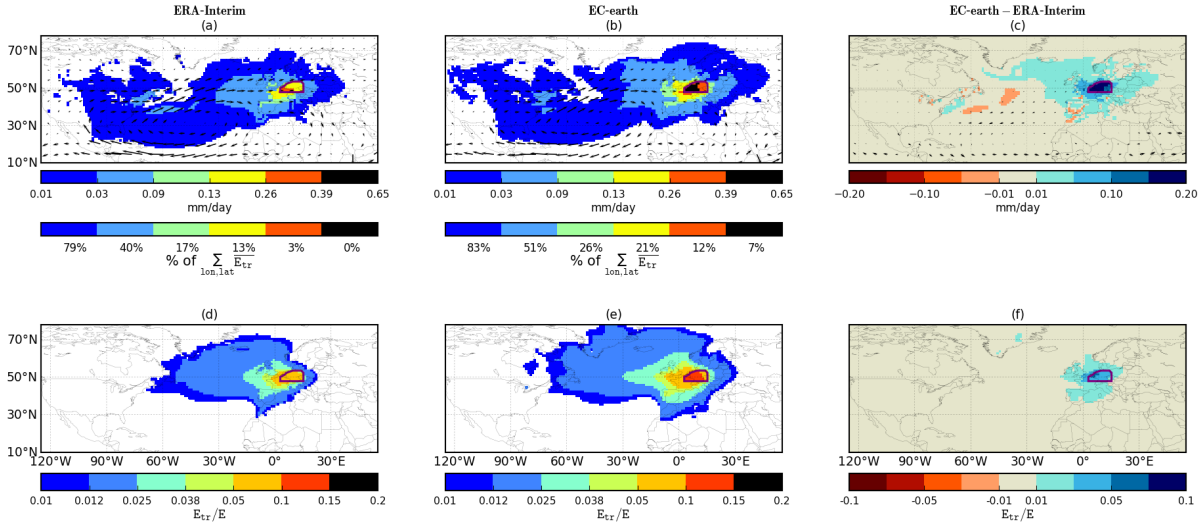

Figure 7: Source of precipitation in region-CEU for JJA (region-CEU is depicted by the purple lining). The values are averaged over 1979 - 2013. The 1st, 2nd and 3rd column represent the data for ERA-Interim, EC-earth and EC-earth - ERA-Interim, respectively. The vectors show the corresponding vertically integrated moisture transport. (a & b) The absolute evaporation-shed, see text in section 3.2 for more information. (c) The climatological difference in source of water precipitating in region CEU in mm/day. (d-g) The evaporation contribution-ratio ($E_{\mathrm{tr}}(lon, lat)/E(lon, lat)$) for region CEU.

winter (Fig. 11b and 12b). Additionally, the land-precipitation metric is used to convey if precipitation has a preference for the water content composition, see method section 2.3. If the land-precipitation metric is positive, then precipitation is more likely to occur in concert with an above average amount of continental water in the atmosphere. In other words, then the link between continental (evaporation) water and precipitation will be stronger.

Combining the information gained from this coupling strength analysis renders evidence that EC-earth simulates a stronger evaporation-precipitation coupling compared to ERA-Interim. To elaborate, EC-earth renders more precipitation from continental origin. This can have multiple causes and an important factor is the amount of continental evaporation, i.e. more continental evaporation leads to more continental water in the atmosphere and hence, more precipitation from continental origin. However, EC-earth is the model simulating a lower amount of continental evaporation (see figure 10). This indicates that EC-earth is rendering more precipitation from continental origin because of the stronger coupling between evaporation and precipitation. Moreover, the land-precipitation metric conveys that (mainly in spring) precipitation is more often occurring when there was an above average amount continental water in the total water column.

A stronger evaporation-precipitation would also explain the evaporation and precipitation bias patterns we observe in summer (fig. 10), because the evaporation-precipitation feedback is enhancing an initial imbalance (amplifying desiccation or moistening). Hence, when soils in spring are drying due to the increased downward radiation ($-\Delta E$), the precipitation can enhance this drying by overestimating the response ($-\Delta P$). Likewise, the wet regions (which are not limited in their evaporation) will become wetter, also because the precipitation will respond too strongly to the (high) evaporation ($+\Delta P$).

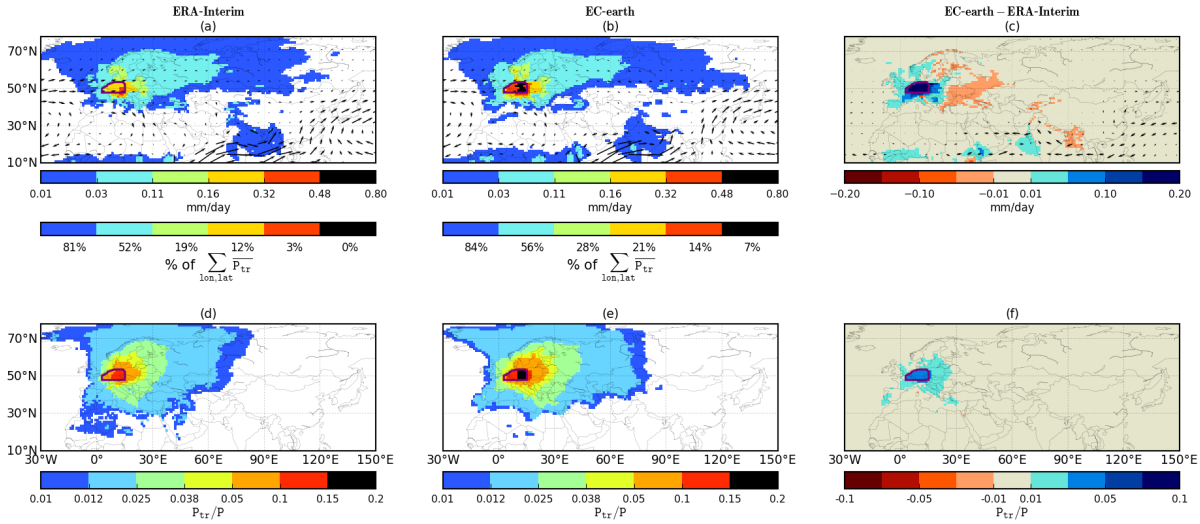

Figure 8: Similar to 7, but now showing the destination of evaporation from the region CEU for JJA. The values are averaged over 1980 - 2014. (a & b) the absolute precipitation-shed. (c) the difference in climatological mean destination of water evaporated in region CEU in mm/day. (d-g) The precipitation contribution-ratio ($P_{\mathrm{tr}}(lon, lat)/P(lon, lat)$).

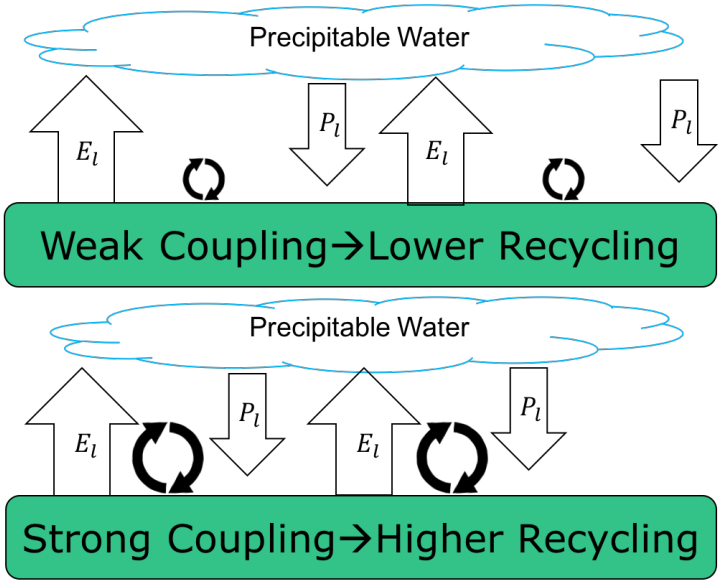

Figure 9: Schematic figure conveying link between moisture recycling and evaporation-precipitation coupling strength. If precipitation is more strongly governed by (local) evaporation, we expect that precipitation events near the evaporation anomaly occur more frequently. Thereby, the amount of precipitation falling nearby the local domain is higher, i.e. a higher local precipitation recycling. On a continental scale, this means that precipitation from continental origin can occur more often, hence, raising the continental recycling ratio.

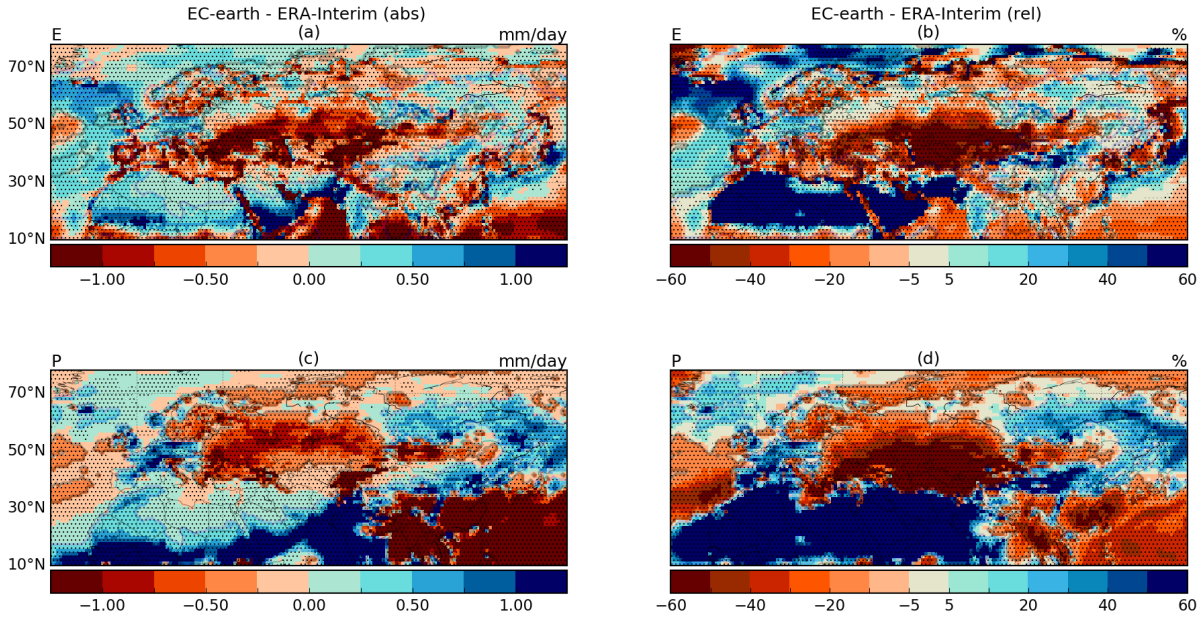

Figure 10: Evaporation and precipitation difference in summer (JJA). Absolute and relative differences in first and second column, respectively.

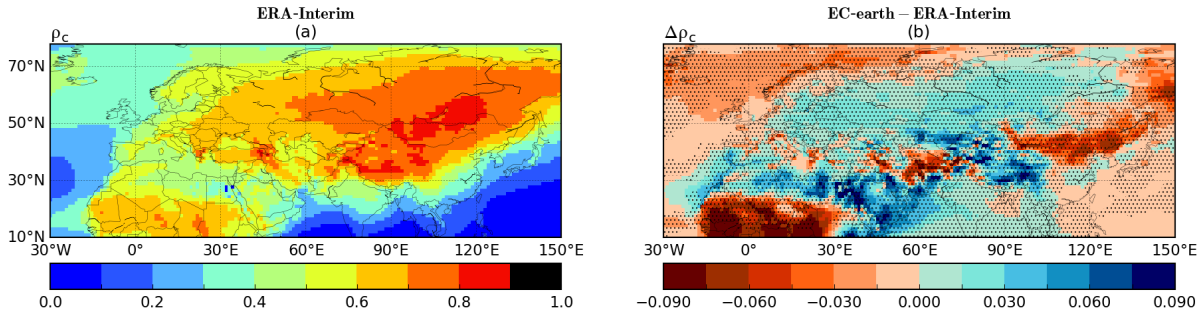

Figure 11: Continental precipitation recycling ratio in summer of ERA-Interim (a), absolute difference, EC-earth − ERA-Interim (b).

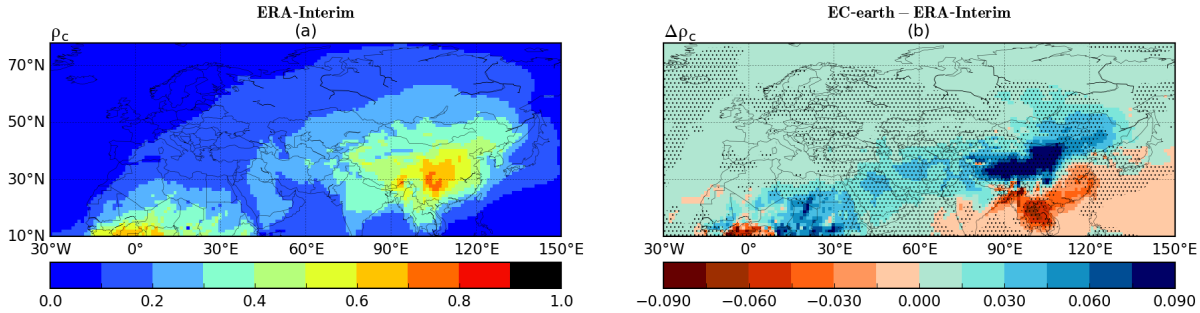

Figure 12: Continental precipitation recycling ratio in winter of ERA-Interim (a), absolute difference, EC-earth − ERA-Interim (b).

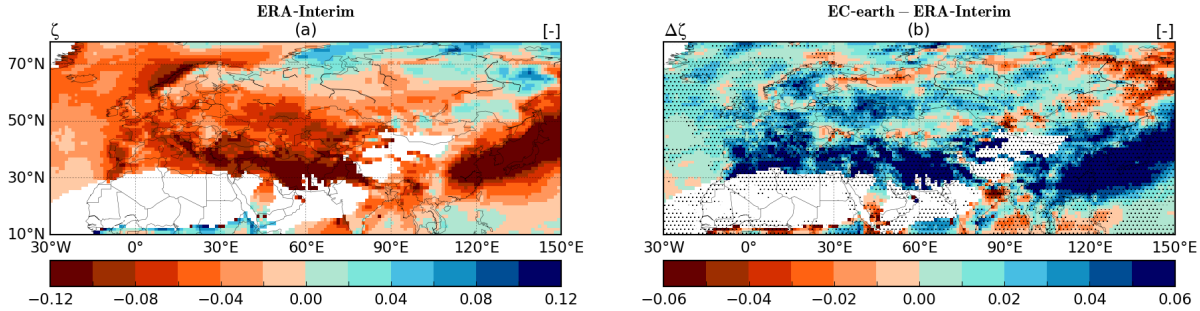

Figure 13: Land-precipitation metric (ζ) in spring (MAM). The zero-hypothesis of the metric is that precipitation has no preference for the water content composition in the atmosphere. If there is more (frequent) precipitation when the amount of continental water is above average, then apparently there is a stronger link between continental water and precipitation (ζ will be positive).

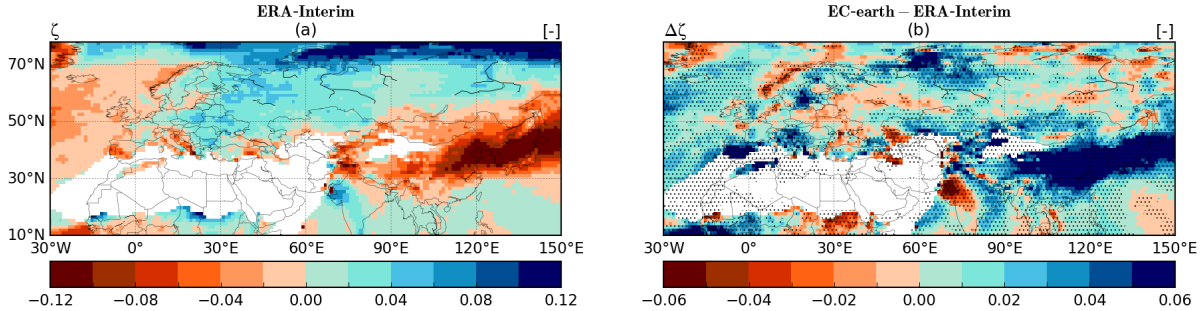

Figure 14: Land-precipitation metric (ζ) in summer (JJA), see caption of figure 13.

4 Results: Surface-runoff Experiment

We dominantly focus on the northern hemisphere to explain the model behavior in response to the surface-runoff formulation, which shows the strongest response due to the large continental land masses. Moreover, the adjustment over large continental land masses is less affected by the variability associated with ocean-land dynamics. Before we discuss the impact of the perturbation on other variables, it is insightful to reveal how the perturbation materialized. In the CTRL-model, surface-runoff only appears when the water content at a timestep exceeds the field capacity, i.e. when soil moisture index (SMI) > 1. Hence, dry regions hardly generate surface-runoff, i.e. the efficiency of the runoff sink (R/P) is generally low in drier regions (see figure 15a and 15b). Since only regions with low R/P are affected by our new formulation, the strongest increase in the runoff sink efficiency (R/P) occurs in these dry regions (see figure 15c).

A (initially) peculiar result of the experiment, is that substantial drying occurred at the peripheries of the perturbation. The drying is plotted for the entire column of the land surface model (0-255 cm, 4 layers) and the top layer (0-7 cm) in figure 16. To clarify the strong dessication at the periphery with respect to the increased runoff-efficiency, we have drawn a red contourline in figure 15c where substantial drying of the entire column occurred. A more detailed discussion on the results can be found in appendix C and D.

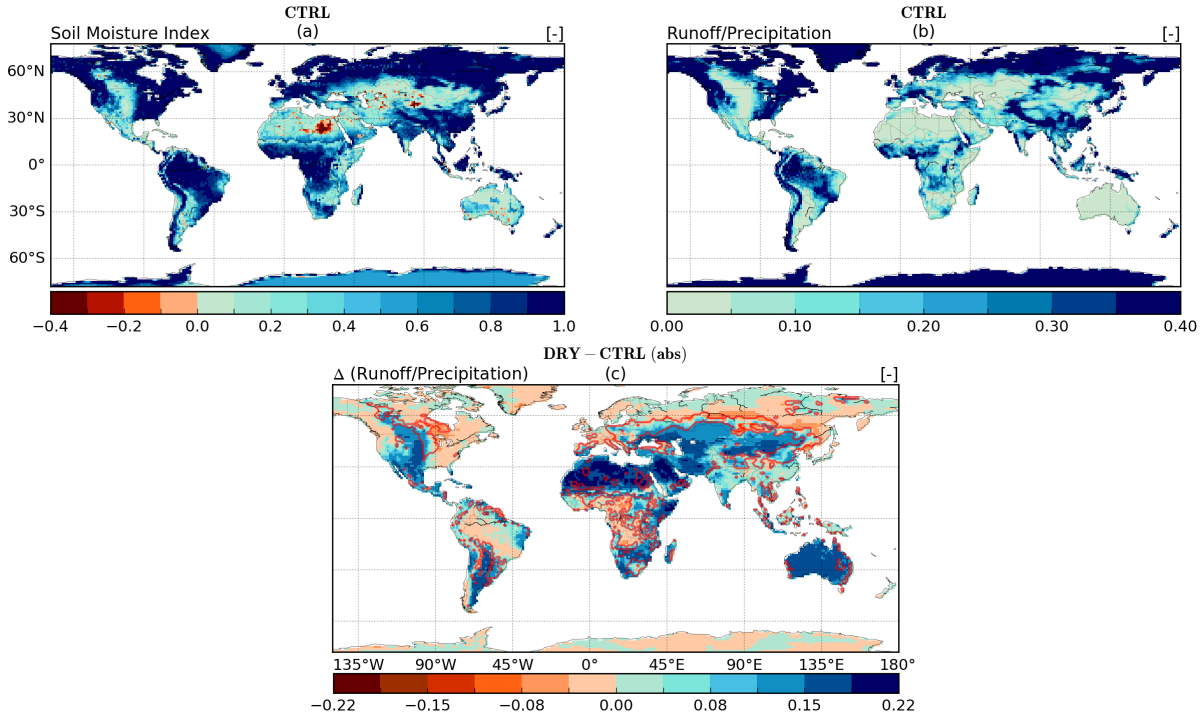

Figure 15: The equilibrium result of the perturbation (annual mean), defined by the increase in runoff-efficiency (R/P) shown in plot (c). Plot (a) shows where the soil moisture content is close to (or below) the wilting point (SMI $\rightarrow$ 0) and where it is close to (or above) the field capacity (SMI $\rightarrow$ 1). Together with plot (b), the link between low soil moisture content and runoff-efficiency can be observed. The red contourlines show where the soil drying over the entire column was at least 20% and significant.

4.1 Large Scale Propagation of Drought

The soil drying, which occurred in regions that are *not* affected (much) by the increased runoff, suggest that the dessication is dominantly forced by a decrease in the precipitation arising in summer (rather then the increase in runoff). The decrease in precipitation is occurring quasi-local (generally downwind) of the evaporation change (see Fig. 17 and appendix C for more detailed information). Thereby clearly visualizing the quasi-local impact of the evaporation-precipitation interaction.

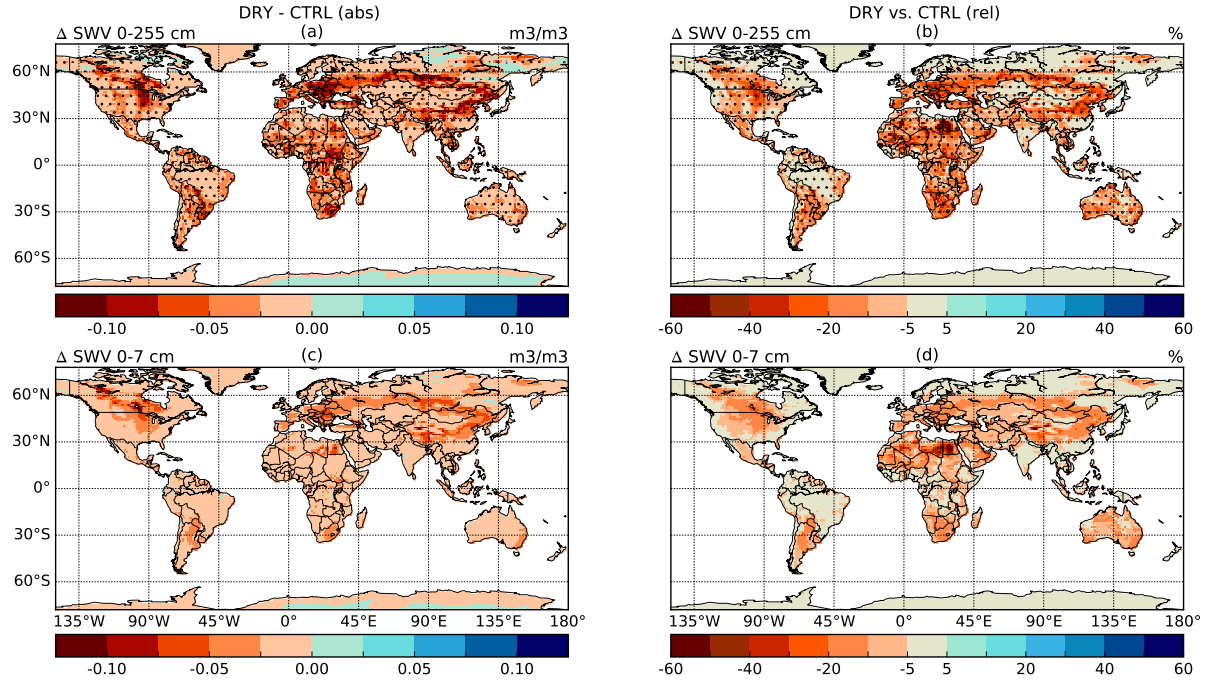

Figure 16: The annual mean soil dessication. (a) and (b) show the absolute and relative change in soil water volume (θ) over all 4 vertical layers. (c) and (d) presents the same, but only for the top layer. The black dots are drawn where the change (DRY-CTRL) exceeds the 95% range of inter-annual variability in the CTRL.

we plot $\Delta P - \Delta E$ to visualize the regions that are (dominantly) desiccated due to a decrease in precipitation, see figure 18. Initially, where the runoff increases, the decrease in evaporation forces an atmospheric adjustment. Subsequently, leading to a decrease in precipitation ΔP, which is (expectedly) less then ΔE. Conversely, where precipitation is driving the desiccation, the soil needs to lower its sinks (runoff and evaporation) by lowering its water content. Note, the runoff indeed decreases in these regions (see figure 20e,f and 21e,f). Since ΔP is split up into a decrease in both a decrease in runoff and evaporation, $|\Delta P| > |\Delta E|$.

The decrease in evaporation also affects the formation of clouds, thereby, enhancing the desiccation. The amount of surface shortwave downward radiation is used as a proxy for the change in cloud cover (figure 19a, b). In the dry regions, such as lower mid-Eurasia, there were hardly clouds present in the CTRL. Hence, it does not have a large impact on the surface solar radiation. Around the peripheries of the perturbation, a significant decrease in cloud cover is observed. The surface air temperature also increases (regionally around $+3°$C, $+15\%$), see figure 29. The increase in temperature is the result of both increased downward surface radiation and altered partitioning of the radiative energy, i.e. less energy is used for evaporating water, hence, more is used for heating the surface (see appendix C.4. The increased surface radiation and temperature both enhance the drying locally and quasi-locally, hence, strengthening the propagation of drought.

4.2 Impact of Reaching Wilting Point

We now know that propagation of drought is driven by the quasi-local decrease in precipitation and clouds. Another interesting aspect is that substantial differences in evaporation, precipitation and temperature between the DRY and CTRL climate only arise in summer, while the relative increase in surface-runoff remains quite constant throughout the year. The absolute increase in runoff actually weakens in summer (see appendix C and D).

We argue that responds to our increased runoff is generally small, *unless* the soil is reaching the wilting point in the DRY, but not the CTRL-run. We plot the SMI (Soil Moisture Index) of the CTRL- and DRY-run to show where the soil water approaches the wilting point (SMI$\rightarrow$0) in figures 20 and 21. In regions where the wilting point is approached in the DRY but not in the CTRL-run, the evaporation decrease is very large compared to the decrease in soil water. In spring however, the soil is still wet and here, thus we do not observe the latter signal

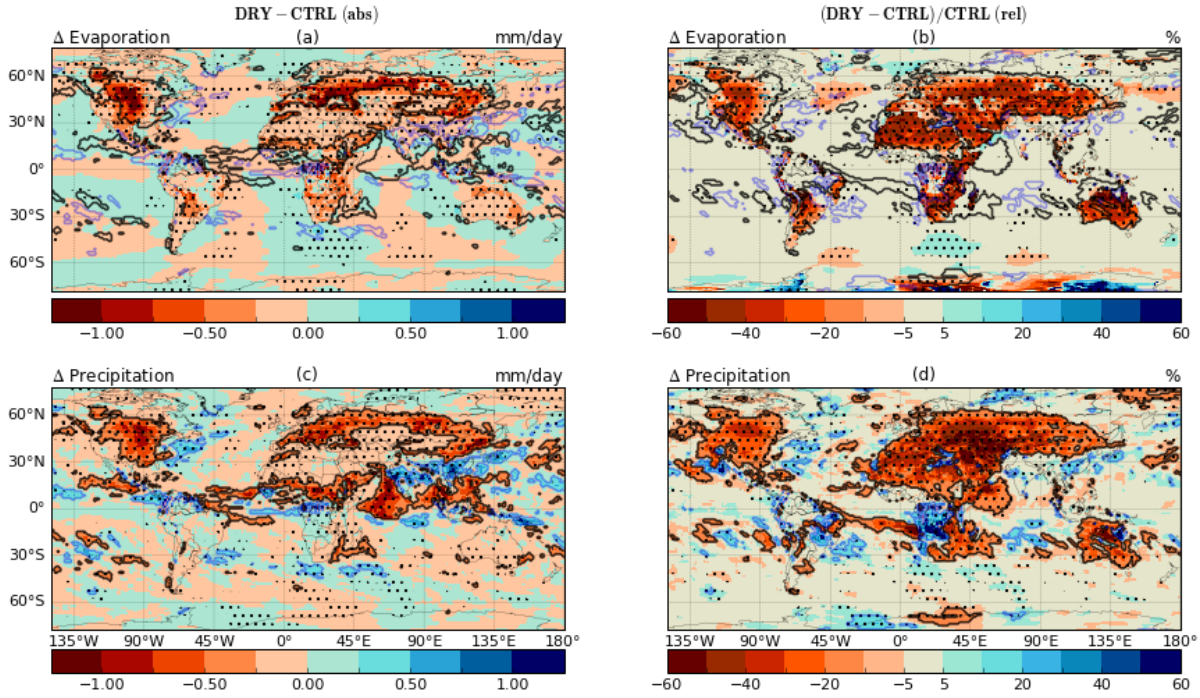

Figure 17: The change in evaporation and precipitation in absolute and relative terms, column 1 and 2 respectively. In the first column, a contourline is plotted in where ΔP¿0.25 mm/day, black (blue) for a negative (positive) change. In the second column, the contourline is drawn where the condition ΔP¿20% is met. These contourlines of precipitation change are also drawn in plots (a) and (b), to show that the precipitation change is occurring quasi-local, i.e. at peripheries of ΔE, and remotely, i.e. around the Inter Tropical Convergence Zone.

(see figure 20). In the DRY-run, the small Δ SWV in summer has caused evaporation to cease completely, leading to a sudden low $\Delta E/\Delta$SWV. This feature is used to show where the DRY-run is reaching the wilting point while the CTRL-run is not. When this criteria is met, we observe the large differences in the evaporation, precipitation and temperature. It demonstrates that small differences in hydrology, which cause the soil water volume to reach the wilting point, can have a large impact on your regional surface conditions. In retrospect, the large impact on evaporation and precipitation inducing the drought propagation, is triggered by the soils reaching the wilting point. Hence, this drought propagation must also be occurring around the regions approaching the wilting point in the CTRL climate.

4.3 Link between Source and Destination of Atmospheric Water

Using the tracking scheme, we observe that continentally evaporated water (referred to as continental water) is transported to specific regions in the atmosphere. Hence, the continental water is accumulating in those regions, generally located above land (see figure 22). Interestingly, there appears to be a clear separation between continental and oceanic water in the atmosphere. Likely related to the fact that land surfaces are generally associated with higher pressure systems, restraining oceanic water to converge land inwards.

In summer, the strongest reduction in evaporation occurs at the peripheries of the perturbation, see figure 17. If there is a link between source and destination, we expect a decrease of continental water in our regions of accumulation (Fig. 22c), referred to as the destination. Figure 22d shows this is true, thereby, proving there is a clear link between source and destination of water.

The atmosphere responds to a decrease in precipitable water and figure 22f shows the equilibrium result of the responds in terms of increased water from oceanic origin. Generally, a strong decrease in continental water shows an associated increase in oceanic water. But, when there is no oceanic water body nearby, the responds of increased oceanic water is restricted. Hence, we observe that above Eurasia and to some extent north-America, the precipitable water decrease is most substantial. Overall, the link between source of water and precipitation is

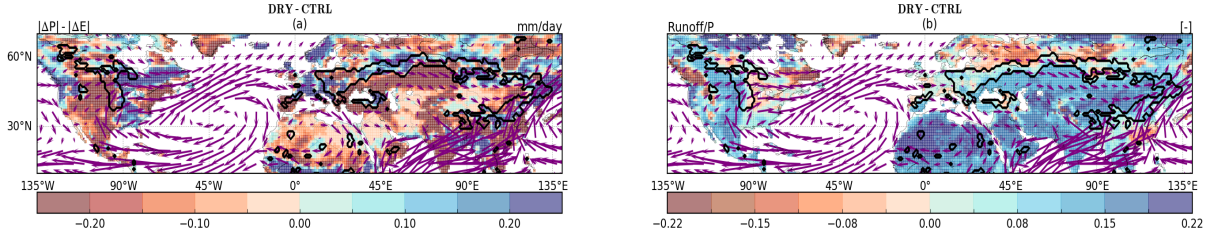

(a) Response in June.

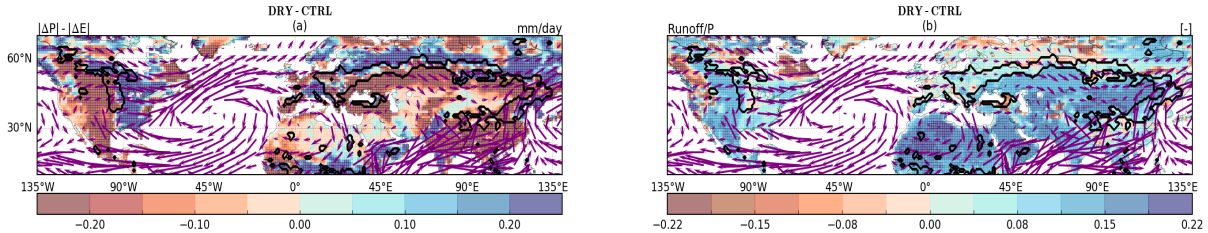

(b) Response in July.

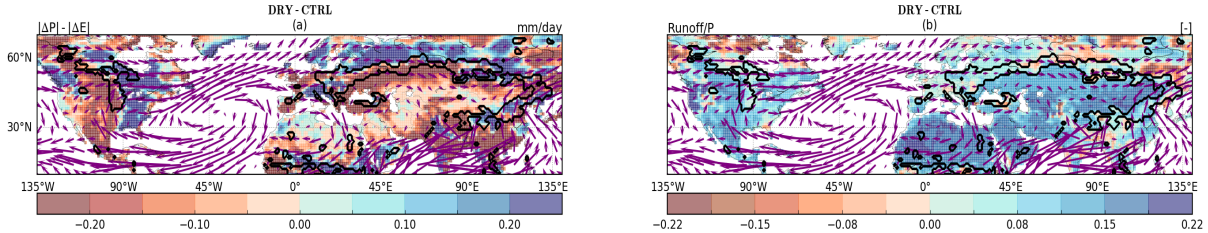

(c) Response in August.

Figure 18: The black contourline shows where the soil drying over the entire column was at least 20% and significant. The purple vectors indicate the climatological moisture flux, mean between DRY and CTRL run. In the second column, we observe that the increase in runoff/P is negligible or even negative at the peripheries throughout June, July and August. The first column shows where precipitation is driving the desiccation, $\Delta P > \Delta E$. As the drying progresses, certain gridcells at the periphery will approach the wilting point, and thereby cease all evaporation (see Fig. 1b). Hence, reaching the wilting point will force a large decrease in evaporation and thereby, $\Delta P < \Delta E$. Conclusively, we are observing propagation of drought driven by the evaporation-precipitation interaction.

dampened by this dynamical adjustment of the atmosphere. The remote change in precipitation appear strongly affected by the cumulative change in precipitable water, i.e. decrease in continental water plus increase in oceanic water.

5 Discussion and Conclusion

This thesis started by elucidating the hydrological performance of the global climate model EC-earth, focusing on Europe. A moisture tracking model compared the source (and destination) of precipitation (evaporation) of EC-earth with ERA-Interim. The accuracy of the evaporation and precipitation-fields from the reanalysis ERA-Interim was deemed insufficient to conclude a significant difference in the absolute precipitation and evaporation-sheds for the region 'Central Europe' (Fig. 8a-c and 7a-c, respectively). However, the moisture recycling ratios are not affected by the absolute biases and it appeared that EC-earth renders a stronger moisture recycling compared to ERA-Interim. We highlighted that a higher moisture recycling is not only associated with a higher amount of continental evaporation accumulating in the atmospheric column aloft, but it is also affected by the evaporation-precipitation coupling. Possibly, the higher moisture recycling in our region 'Central Europe', is caused by a stronger evaporation-precipitation coupling of EC-earth with respect to ERA-Interim. Note, due to the large inconsistencies of ERA-Interim, this does not mean that EC-earth overestimates the moisture recycling

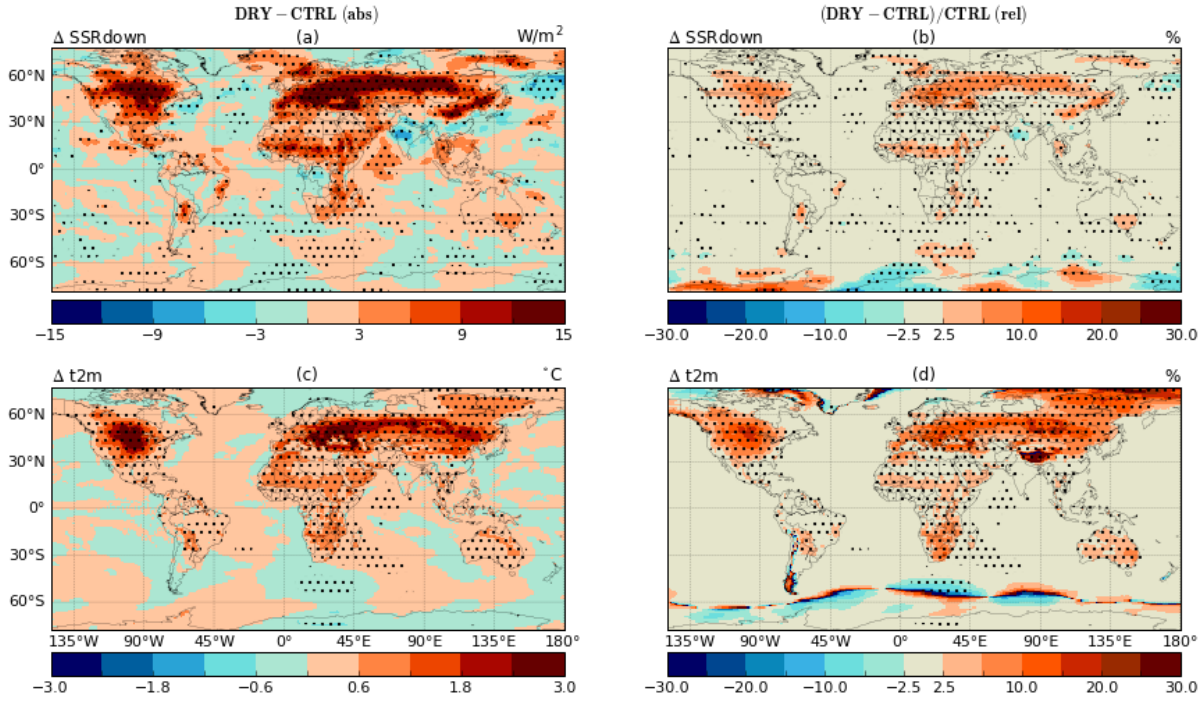

Figure 19

with respect to reality.

Successively, we attempted to evaluate the evaporation-precipitation coupling on a larger spatial scale, i.e. over Eurasia. We analyzed evaporation and precipitation fields and quantified how much precipitation was originating from continental evaporation. Furthermore, we introduced a new land-precipitation metric, where the zero-hypothesis states that precipitation has no preference for the atmospheric water content composition. If there is more precipitation when there is an above average amount of continental water in the atmosphere, then apparently, precipitation is more strongly influenced by continental water. The land-precipitation metric is further evaluated in appendix E and captures the expected features, such as the increased coupling strength between evaporation and precipitation in summer, and near the coasts, more precipitation in concert with high oceanic water content.

The evaporation-precipitation coupling analyses provided evidence that EC-earth is rendering a stronger evaporation-precipitation coupling. To elaborate, despite the fact that ERA-Interim simulated more continental evaporation, thereby increasing the water content from continental origin, the continental precipitation recycling ratio was still found to be lower. In other words, the precipitation originating from continental evaporation played a more important role in EC-earth compared to ERA-Interim. Furthermore the land-precipitation metric showed that, especially in spring, precipitation in EC-earth is more often occurring in concert with a high amount of continental water in the atmosphere, see figure 11 and 14. These lines of evidence combined indicate that EC-earth is rendering more precipitation from continental origin because of the stronger coupling between evaporation and precipitation. The stronger coupling could be related to the minor adjustments in the atmospheric model with respect to ERA-Interim or the fact that ERA-Interim is constrained by observations to a lesser role of oceanic evaporation simulated by the coupled ocean model (only present in the EC-earth model). In appendix A, we present more details on the differences between EC-earth and ERA-Interim.

A stronger evaporation-precipitation coupling means that precipitation events are more strongly influenced by evaporation. If we regard this issue in a seasonal cycle context, we expect the observed bias patterns as seen in summer comparing EC-earth with ERA-Interim, see figure 10. To elaborate, when moisture-limited soil regimes in spring are drying due to the increased downward radiation ($-\Delta E$), the precipitation can enhance this drying by overestimating the response ($-\Delta P$). Conversely, in energy-limited soil regimes, see figure 1, the evaporation will increase in spring due to increased radiation. In wet regions the precipitation will respond too strongly to the increased evaporation, leading to a positive bias with respect to the model simulating a weaker

evaporation-precipitation coupling ($+\Delta P$), this confirmed in figure 10. The same systematic evaporation and precipitation bias patterns are observed in CMIP5-models (Mueller and Seneviratne, 2014), see figure 2. These biases in evaporation lead to temperature overestimations (underestimation) in dry (wet) regions, also shown in Mueller and Seneviratne (2014). In fact, the latter temperature bias pattern is also a known problem in regional climate models (Davin et al., 2016).

The overestimation of the evaporation-precipitation coupling with respect to reality is supported by model experiments (Hohenegger et al., 2009; Taylor et al., 2013) and observations Taylor et al. (2012). Satellite measurements of soil moisture and precipitation are implemented to show that afternoon rainfalls were more often preceded by dry soils compared to its surroundings (Taylor et al., 2012), indicating a negative soil moisture-precipitation feedback. However, the same analysis in several global climate models shows that a positive feedback dominates, less (more) precipitation over dry (wet) soils. Taylor et al. (2012) already noted that this could contribute to "the excessive simulated droughts in large-scale models". Modeling experiments hint at the role of inaccurate convection generated by parametrization in regional and global climate models. Taylor et al. (2013); Hohenegger et al. (2009) show that parametrized convection leads to a (strong) positive soil moisture-precipitation feedback, while explicitly resolving convection can render a negative feedback. The flaw of the parametrized convection lies in its inability to resolve vigorous thermals which can break through the stable air barrier (and thereby trigger deep-convection) (Hohenegger et al., 2009). Our analysis comparing EC-earth with ERA-Interim (section 3.3), provides evidence that a stronger evaporation-precipitation coupling will indeed lead to excessive drought (and also excessive precipitation over wet regions).

Successive to the evaporation-precipitation coupling analysis, we analyzed an experiment where the runoff sink was made more efficient only in (semi-) dry regions. This heterogeneous perturbation visualized how evaporation was affecting precipitation non-locally. In our experiment, the strongest dessication was observed at the periphery of where the perturbation materialized (see figure 16), i.e. in those regions there was no increase in runoff. In the 'perturbed regions' during fall, winter and spring, the increased runoff did render stronger desiccation in the (semi-) dry regions (not shown). But, when the soil water content approaches the wilting point in summer, the soil starts to prohibit evaporation. The associated large decrease in evaporation, induces a strong response in precipitation, clouds and surface conditions (see section 4.2). We presented this section to clarify that reaching the wilting point in summer has a severe impact on the response. We are doubtful about at the realism of suddenly ceasing all evaporation (see figure 1b), perhaps the yearly cycle of soil moisture would be more accurate by making the limitation of evaporation continuous.

As a result of the large decrease in evaporation in summer, the quasi-local strong decrease in precipitation and clouds is propagating drought on a large scale (see section 4.1). In section 4.1, we show that desiccated soils can induce a strong quasi-local effect via the evaporation-atmosphere interactions. In fact, the evaporation and precipitation pattern associated with drought propagation (too low evaporation in dry regions, surrounded downwind by too low precipitation) can be observed in the mean of CMIP-5 Global Climate Models (Fig. 2) and similarly in our comparison between EC-earth and ERA-Interim (Fig. 10).

The propagation of drought is also identified in observations over Europe (Vautard et al., 2007), where the 10 most intense European heat waves were preceded by significant rainfall deficits in southern Europe. The proposed mechanisms for the northward propagation of (heat) drought in observations were confirmed and detailed by the work of Zampieri et al. (2009). In hind sight, the experiment performed by Zampieri et al. (2009) over Europe is qualitatively similar to our experiment. The regional study of Zampieri et al. (2009) focused on Europe and the desiccating perturbation was only implemented across southern Europe. South 46°, the volumetric soil moisture was artificially set to 15% in the DRY experiment and 30% in the WET experiment. The transient evolution of the summer season was a northward propagation of the drought. Likewise, Zampieri et al. (2009) proposed the decrease in 'precipitation potential' of the air due to lowered humidity, increase in radiation (due to lowered cloud cover) enhances the drying northward of the perturbation. Moreover, he noted these two affects also render an increase in temperature, thereby favoring the formation of stagnant weather.

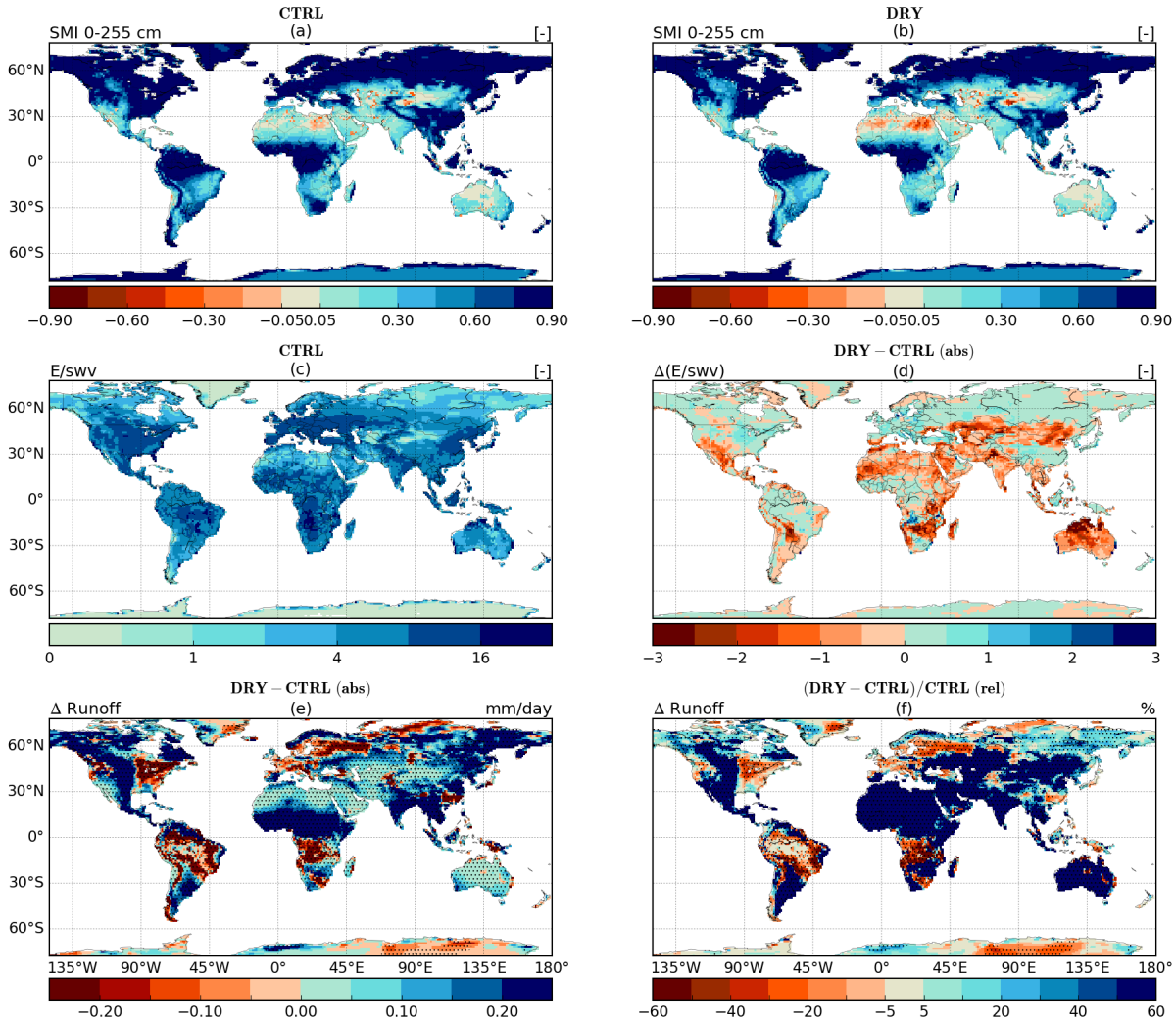

Figure 20: The soil moisture index of the DRY and CTRL run in May are shown in plot (a) and (b), respectively. (c) shows the evaporation efficiency with respect to its volumetric soil water content in the CTRL. (d) shows the change (DRY-CTRL) in the latter value. (e) and (f) show the change in runoff in absolute and relative terms, respectively.

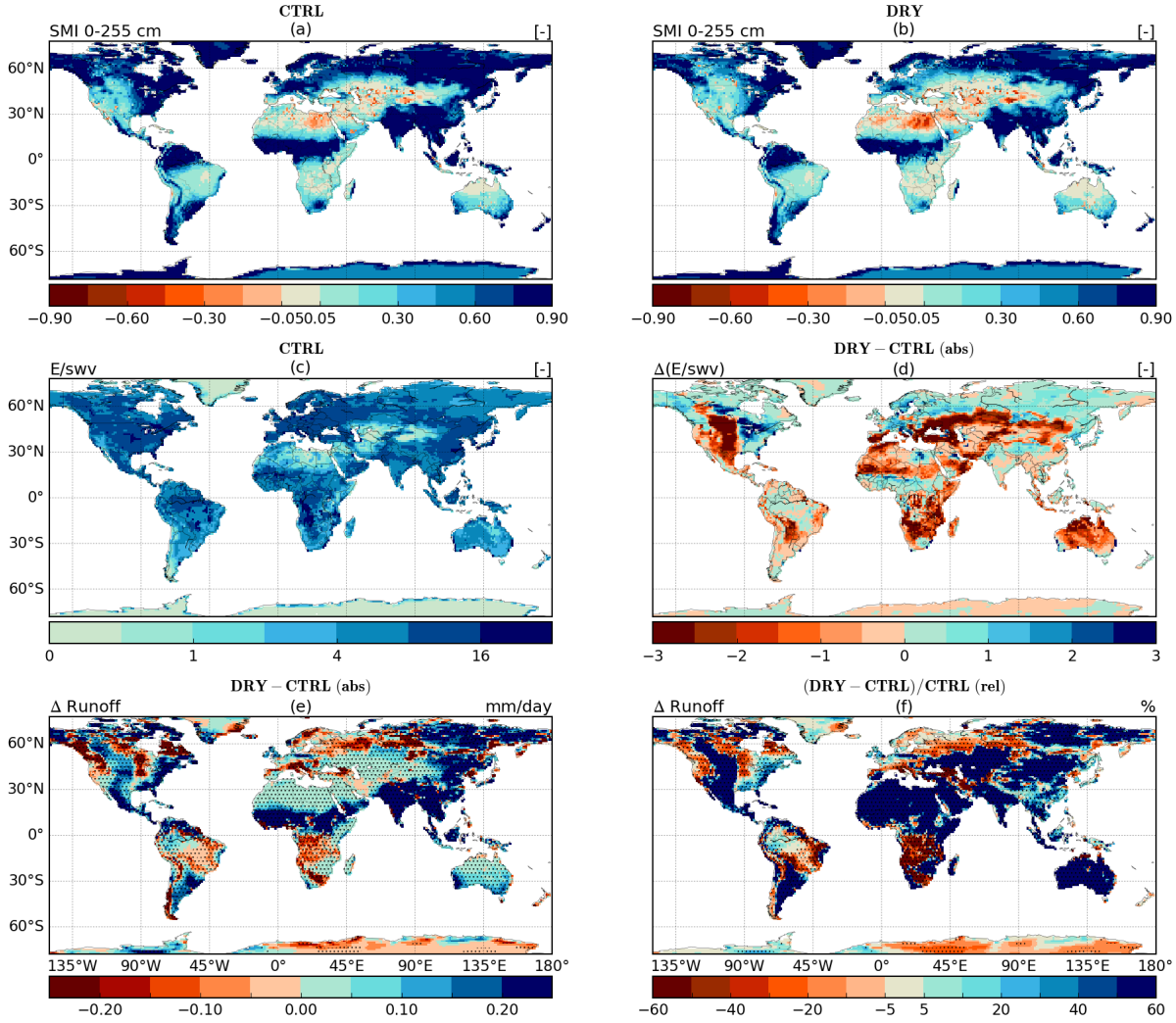

Figure 21: Same as figure 20, but for July. In plot (a) and (b) we observe that more regions are approaching the wilting in the DRY-run with respect to the CTRL-run. The runoff perturbation has actually decreased compared to spring, plot (e) and (f), but the decrease in evaporation is suddenly getting much larger, in appendix C and D, the responds in summer and spring are presented, respectively. With plot (d), we show that this sudden strong responds is associated with soils reaching of the wilting point, see text.

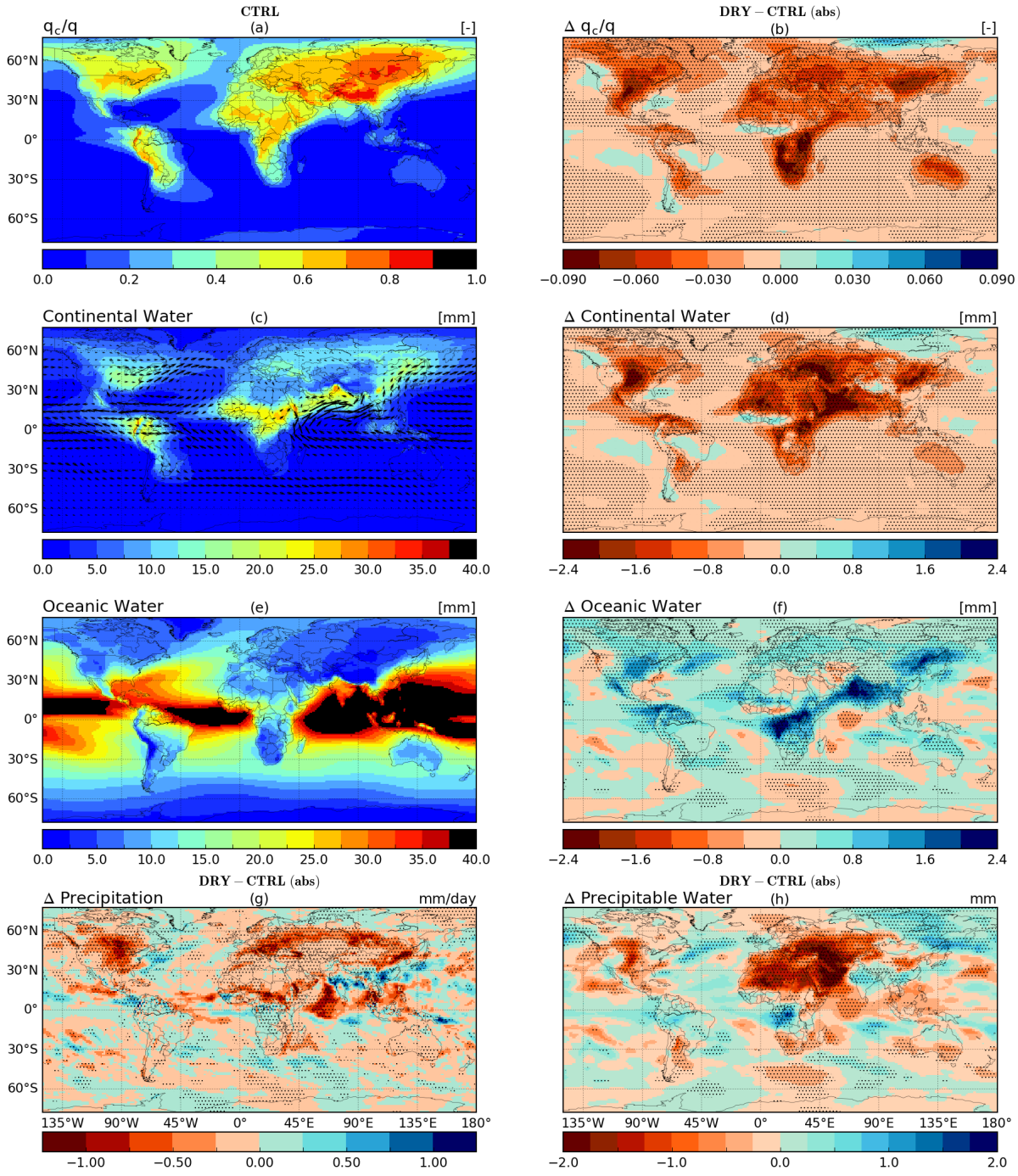

Figure 22: Result of tracking water, split into continental and oceanic evaporated water in summer. (a, c, e) The role of evaporation from oceans or continents in the atmospheric water content. (b) The change in water content composition (q_c/q) and (d, f) the change in individual sources [mm]. (h) displays the change in the total atmospheric water content [Δmm]. (g) the change in precipitation is plotted to smoothen evaluation with the changes in the atmospheric water content.

6 Outlook

It has to be said that (semi-)dry regions (below field capacity) are inherently prone to a greater uncertainty in dessication due to their dependence on precipitation, which caries its own uncertainty. However, we speculate that the summer underestimation in evaporation and precipitation in dry regions as simulated by global climate models, is partly due to an overestimation of the evaporation-precipitation coupling. This overestimation of evaporation-precipitation coupling would also explain the overestimation of precipitation over wet regions. Additionally, it will also affect the drought propagation we identified around dry regions.

To robustly test to what extent the 'overestimation of summer-desiccation in semi-dry regions' is indeed a feature (partly) caused by the evaporation-precipitation coupling, we propose to analyze the difference of a full year simulation with parametrized and explicit convection. It would also be interesting to test if the northward propagation would still be as strong when the domain is explicitly resolving convection. A combination of the simulation by Zampieri et al. (2009) and Hohenegger et al. (2009) will provide us the answer to both questions with one experiment.

References

Adler, R. F., Huffman, G. J., Chang, A., Ferraro, R., Xie, P.-P., Janowiak, J., Rudolf, B., Schneider, U., Curtis, S., Bolvin, D., Gruber, A., Susskind, J., Arkin, P., and Nelkin, E. (2003). The Version-2 Global Precipitation Climatology Project (GPCP) Monthly Precipitation Analysis (1979–Present). *Journal of Hydrometeorology*, 4(6):1147–1167.

Balsamo, G., Beljaars, A., Scipal, K., Viterbo, P., van den Hurk, B., Hirschi, M., and Betts, A. K. (2009). A Revised Hydrology for the ECMWF Model: Verification from Field Site to Terrestrial Water Storage and Impact in the Integrated Forecast System. *Journal of Hydrometeorology*, 10(3):623–643.

Berrisford, P., Dee, D., Fielding, K., Fuentes, M., Kallberg, P., Kobayashi, S., and Uppala, S. (2009). The ERA-Interim Archive. *ERA report series*, 1(1):1–16.

Boberg, F. and Christensen, J. H. (2012). Overestimation of Mediterranean summer temperature projections due to model deficiencies. *Nature Climate Change*, 2(6):433–436.

Davin, E. L., Maisonnave, E., and Seneviratne, S. I. (2016). Is land surface processes representation a possible weak link in current Regional Climate Models ? *Environmental Research Letters*, 11(7):1–8.

Dee, D. P., Uppala, S. M., Simmons, A. J., Berrisford, P., Poli, P., Kobayashi, S., Andrae, U., Balmaseda, M. A., Balsamo, G., Bauer, P., Bechtold, P., Beljaars, A. C. M., van de Berg, L., Bidlot, J., Bormann, N., Delsol, C., Dragani, R., Fuentes, M., Geer, A. J., Haimberger, L., Healy, S. B., Hersbach, H., Hólm, E. V., Isaksen, L., Kållberg, P., Köhler, M., Matricardi, M., Mcnally, A. P., Monge-Sanz, B. M., Morcrette, J. J., Park, B. K., Peubey, C., de Rosnay, P., Tavolato, C., Thépaut, J. N., and Vitart, F. (2011). The ERA-Interim reanalysis: Configuration and performance of the data assimilation system. *Quarterly Journal of the Royal Meteorological Society*, 137(656):553–597.

Dirmeyer, P. A. and Brubaker, K. L. (2007). Characterization of the Global Hydrologic Cycle from a Back-Trajectory Analysis of Atmospheric Water Vapor. *Journal of Hydrometeorology*, 8(1):20–37.

ECMWF (2011). IFS DOCUMENTATION – Cy37r2 Operational implementation 18 May 2011 PART IV : PHYSICAL PROCESSES. *ECMWF IFS documentation*, (May):1–174.

Feser, F., Rockel, B., von Storch, H., Winterfeldt, J., and Zahn, M. (2011). Regional Climate Models Add Value to Global Model Data: A Review and Selected Examples. *Bulletin of the American Meteorological Society*, 92(9):1181–1192.

Fischer, E. M., Seneviratne, S. I., Vidale, P. L., Lüthi, D., and Schär, C. (2007). Soil moisture-atmosphere interactions during the 2003 European summer heat wave. *Journal of Climate*, 20(20):5081–5099.

Goessling, H. F. and Reick, C. H. (2011). What do moisture recycling estimates tell us? Exploring the extreme case of non-evaporating continents. *Hydrology and Earth System Sciences*, 15(10):3217–3235.

Haarsma, R. J., Selten, F., Hurk, B. V., Hazeleger, W., and Wang, X. (2009). Drier Mediterranean soils due to greenhouse warming bring easterly winds over summertime central Europe. *Geophysical Research Letters*, 36(4):1–7.

Hazeleger, W., Severijns, C., Semmler, T., Ştefănescu, S., Yang, S., Wang, X., Wyser, K., Dutra, E., Baldasano, J. M., Bintanja, R., Bougeault, P., Caballero, R., Ekman, A. M. L., Christensen, J. H., Van Den Hurk, B., Jimenez, P., Jones, C., Kållberg, P., Koenigk, T., McGrath, R., Miranda, P., Van Noije, T., Palmer, T., Parodi, J. A., Schmith, T., Selten, F., Storelvmo, T., Sterl, A., Tapamo, H., Vancoppenolle, M., Viterbo, P., and Willén, U. (2010). EC-Earth: A seamless Earth-system prediction approach in action. *Bulletin of the American Meteorological Society*, 91(10):1357–1363.

Hazeleger, W., Wang, X., Severijns, C., Ştefănescu, S., Bintanja, R., Sterl, A., Wyser, K., Semmler, T., Yang, S., van den Hurk, B., van Noije, T., van der Linden, E., and van der Wiel, K. (2012). EC-Earth V2.2: Description and validation of a new seamless earth system prediction model. *Climate Dynamics*, 39(11):2611–2629.

Hohenegger, C., Brockhaus, P., Bretherton, C. S., and Schär, C. (2009). The soil moisture-precipitation feedback in simulations with explicit and parameterized convection. *Journal of Climate*, 22(19):5003–5020.

Keys, P. W., Barnes, E. A., Van Der Ent, R. J., and Gordon, L. J. (2014). Variability of moisture recycling using a precipitationshed framework. *Hydrology and Earth System Sciences*, 18(10):3937–3950.

Kleidon, a. and Heimann, M. (2000). Assessing the role of deep rooted vegetation in the climate system with model simulations: mechanism, comparison to observations and implications for Amazonian deforestation. *Climate Dynamics*, 16:183–199.

Lintner, B. R. and Neelin, J. D. (2009). Soil Moisture Impacts on Convective Margins. *Journal of Hydrometeorology*, 10(4):1026–1039.

Lorenz, R., Arg??eso, D., Donat, M. G., Pitman, A. J., Van Den Hurk, B., Berg, A., Lawrence, D. M., Ch??ruy, F., Ducharne, A., Hagemann, S., Meier, A., Milly, P. C. D., and Seneviratne, S. I. (2016). Influence of land-atmosphere feedbacks on temperature and precipitation extremes in the GLACE-CMIP5 ensemble. *Journal of Geophysical Research: Atmospheres*, 121(2):607–623.

Martens, B., Miralles, D. G., Lievens, H., van der Schalie, R., de Jeu, R. A. M., Férnandez-Prieto, D., Beck, H. E., Dorigo, W. A., and Verhoest, N. E. C. (2016). GLEAM v3: satellite-based land evaporation and root-zone soil moisture. *Geoscientific Model Development Discussions*, (August):1–36.

Mintz, J. S. Y. (1982). Influence of Land-Surface Evapotranspiration on the Earth's Climate. *Science*, 215(4539):1498–1501.

Mueller, B. and Seneviratne, S. I. (2014). Systematic land climate and evapotranspiration biases in CMIP5 simulations. *Geophysical Research Letters*, 41(1):128–134.

Reichler, T. and Kim, J. (2008). How well do coupled models simulate today's climate? *Bulletin of the American Meteorological Society*, 89(3):303–311.

Santanello, J. A., Peters-Lidard, C. D., Kumar, S. V., Alonge, C., and Tao, W.-K. (2009). A Modeling and Observational Framework for Diagnosing Local Land–Atmosphere Coupling on Diurnal Time Scales. *Journal of Hydrometeorology*, 10(3):577–599.

Seneviratne, S. I., Corti, T., Davin, E. L., Hirschi, M., Jaeger, E. B., Lehner, I., Orlowsky, B., and Teuling, A. J. (2010). Earth-Science Reviews Investigating soil moisture – climate interactions in a changing climate : A review. *Earth Science Reviews*, 99(3-4):125–161.

Seneviratne, S. I., Wilhelm, M., Stanelle, T., Van Den Hurk, B., Hagemann, S., Berg, A., Cheruy, F., Higgins, M. E., Meier, A., Brovkin, V., Claussen, M., Ducharne, A., Dufresne, J. L., Findell, K. L., Ghattas, J., Lawrence, D. M., Malyshev, S., Rummukainen, M., and Smith, B. (2013). Impact of soil moisture-climate feedbacks on CMIP5 projections: First results from the GLACE-CMIP5 experiment. *Geophysical Research Letters*, 40(19):5212–5217.

Sippel, S., Zscheischler, J., Mahecha, M. D., Orth, R., Reichstein, M., Vogel, M., and Seneviratne, S. I. (2017). Refining multi-model projections of temperature extremes by evaluation against land-Atmosphere coupling diagnostics. *Earth System Dynamics*, 8(2):387–403.

Taylor, C. M., Birch, C. E., Parker, D. J., Dixon, N., Guichard, F., Nikulin, G., and Lister, G. M. S. (2013). Modeling soil moisture-precipitation feedback in the Sahel: Importance of spatial scale versus convective parameterization. *Geophysical Research Letters*, 40(23):6213–6218.

Taylor, C. M., Jeu, D., Richard, a. M., Guichard, F., Harris, P. P., and Dorigo, W. a. (2012). Afternoon rain more likely over drier soils. *Nature*, 489(7416):423–426.

Teuling, A. J. and Seneviratne, S. I. (2008). Contrasting spectral changes limit albedo impact on land-atmosphere coupling during the 2003 European heat wave. *Geophysical Research Letters*, 35(3).

Trenberth, K. E., Fasullo, J. T., and Mackaro, J. (2011). Atmospheric moisture transports from ocean to land and global energy flows in reanalyses. *Journal of Climate*, 24(18):4907–4924.

van der Ent, R. J. (2014). *A new view on the hydrological cycle over continents.*

van der Ent, R. J. (2016). WAM2layersPython.

Van Der Ent, R. J. and Savenije, H. H. G. (2011). Length and time scales of atmospheric moisture recycling. *Atmospheric Chemistry and Physics*, 11(5):1853–1863.

Van Der Ent, R. J., Savenije, H. H. G., Schaefli, B., and Steele-Dunne, S. C. (2010). Origin and fate of atmospheric moisture over continents. *Water Resources Research*, 46(9):1–12.

Van Der Ent, R. J., Tuinenburg, O. A., Knoche, H. R., Kunstmann, H., and Savenije, H. H. G. (2013). Should we use a simple or complex model for moisture recycling and atmospheric moisture tracking? *Hydrology and Earth System Sciences*, 17(12):4869–4884.

Vautard, R., Yiou, P., D'Andrea, F., de Noblet, N., Viovy, N., Cassou, C., Polcher, J., Ciais, P., Kageyama, M., and Fan, Y. (2007). Summertime European heat and drought waves induced by wintertime Mediterranean rainfall deficit. *Geophysical Research Letters*, 34(7):1–5.

Zampieri, M., D'Andrea, F., Vautard, R., Ciais, P., De Noblet-Ducoudré, N., and Yiou, P. (2009). Hot European summers and the role of soil moisture in the propagation of mediterranean drought. *Journal of Climate*, 22(18):4747–4758.

A Model specifications

The ERA-Interim reanalysis is developed at the European Center for Medium Range Weather Forecasting (ECWMF). EC-earth is the result of European collaboration to build an Earth System Model and benefits from model development done at the ECMWF. Therefore, the similarities (of the atmospheric and land surface model) are high, see table 1.

The tuned version of the EC-earth atmospheric model consists of improved 1. entrainment description in deep convection, 2. cloud optical thickness description and 3. mass conservation. The land surface scheme TESSEL of EC-earth contains revised soil hydrology conductivity, diffusivity and surface run-off. The snow scheme was also improved in terms of albedo, timing of run-off (melt) and variation in terrestrial water storage.

Table 1: Specification of EC-earth and ERA-Interim. For more information on EC-earth: Hazeleger et al. (2012, 2010), and ERA-Interim Berrisford et al. (2009); Dee et al. (2011) and consult the IFS Documentation here. 4D-VAR and OI are two different analysis methods and TYPE A and TYPE B refer to variables directly constraint by observation and indirectly constrained by observations, respectively.

	EC-earth v2.2	**ERA-Interim**
Atmospheric model	tuned IFS cy31r2	IFS cy31r2
Ocean model	NEMO v2	N/A
Ocean wave model	N/A	ERA Interim Wave
Land Surface Scheme	tuned TESSEL	TESSEL
Sea Ice Model	LIM2	N/A
Analysed	Free model run	4D-VAR TYPE A: u, v, T, q, O3, SP, OI TYPE A: T2m, d2m, 1D-VAR: tcwv TYPE B: soil moisture & temp.

B Evaporation and Precipitation from Observations

To provide more context concerning the presented biases in e.g. section 3.1, we present the global evaporation field of the GLEAM v3 dataset and precipitation from the GPCP v2.3 project.

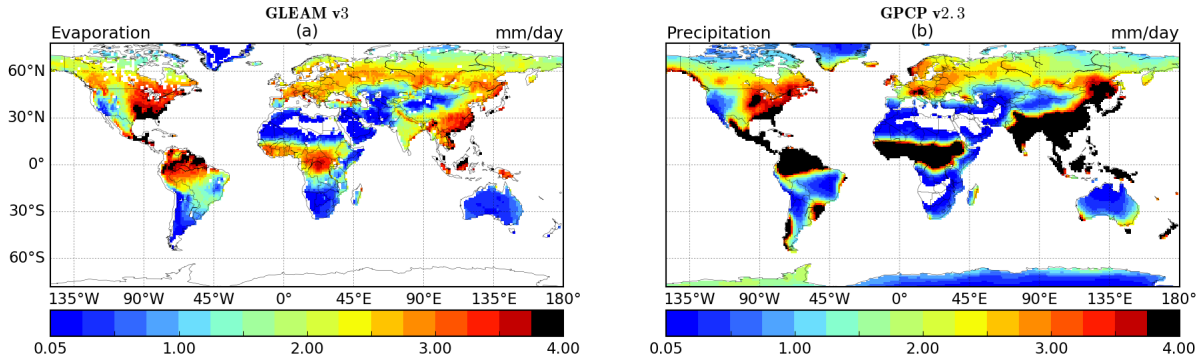

Figure 23: Climatological (1980-2010) evaporation and precipitation from observation(-based) datasets in summer (JJA), see method section 2.4.1. The Global Land Evaporation Amsterdam Model (GLEAM) version 3 is used for evaporation and Global Precipitation Climatology Project (GPCP) version 2.3 is used for precipitation.

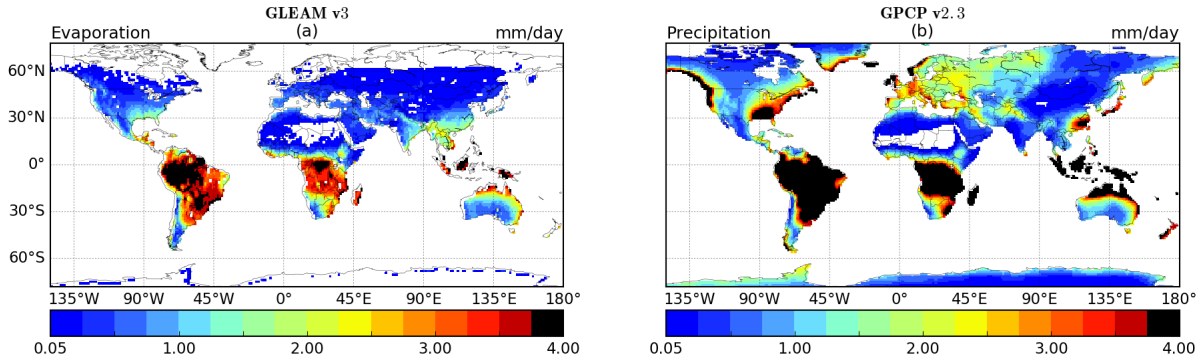

Figure 24: Climatological (1980-2010) evaporation and precipitation from observation(-based) datasets in winter (DJF), see caption figure 23.

C Model response to SRO perturbation in summer

C.1 Perturbation (summer)

The most substantial response occurs in summer. The following description of the soil hydrology and atmospheric hydrology response will explain why the perturbation is strongest at the peripheries. For completeness, we now present the equilibrium effect of the perturbation in summer, albeit, it does not differ much from the annual mean (see figure 25).

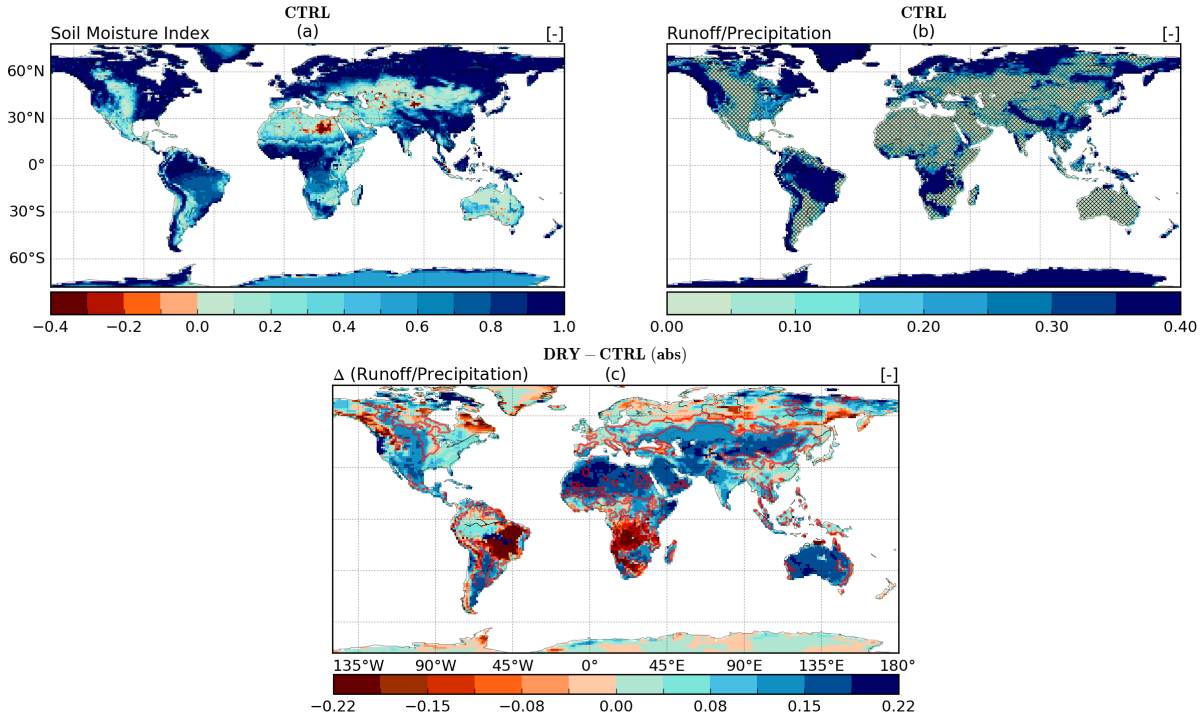

Figure 25: The equilibrium result of the perturbation in summer (JJA)), defined by the increase in Runoff-efficiency (R/P) shown in plot (c). Plot (a) shows where the soil moisture content is close to (or below) the wilting point (SMI $\rightarrow$ 0) and where it is close to (or above) the field capacity (SMI $\rightarrow$ 1). Together with plot (b), the link between low soil moisture content and runoff-efficiency can be observed. The red contourlines show where the soil drying over the entire column was at least 20% and significant.

C.2 Soil Hydrology (summer)

The change in soil water volume (θ) due to the adapted surface-runoff description is shown in figure 26(a, b). Over almost all the continents, the soil water volume decreases. The signal of dessication vertically integrated over all 4 layers is significant and hardly shows seasonality. The top surface layer (0-7 cm), however, is showing stronger seasonality, as expected, compared to the vertically integrated dessication (see the drying of the soil in spring in figure 31 and annually in figure 16). The higher variability in the top layer is likely the reason that the dessication is non-significant.

The low decrease in soil water (and actually moistening) in dry regions can be explained by the fact that dry soils at the wilting point prohibit evaporation. If climatologically the surface-runoff would dessicate the soil close to the (permanent) wilting point (θ_{wpw}), the soil would (more often) prohibit (bare soil) evaporation. This provides a strong negative feedback when the soil is exposed to a desiccating perturbation. The dominant water sink (evaporation) will cease and the soil dessication will even moisten. That the evaporation is the dominant sink in dry soil is trivial when recalling the water mass balance,

$$P = TRO + E \rightarrow 1 = \frac{RO}{P} + \frac{E}{P}, \tag{9}$$

indicating that when the surface-runoff sink (R/P) is inefficient, the evaporative sink (E/P) must be efficient. The fact that the peripheries experience a substantial drying despite a low perturbation becomes clear when examining the atmospheric hydrological response (see next section). The latter will also explain why, in some regions, runoff increases substantially (see figure 26e, f).

Trivially, the drying of the soil ($P-E-RO<0$) in the northern hemisphere occurs in spring and summer. In Appendix **??**, the DRY-run show experiences an intensification of dessication from fall to spring in the 'perturbed regions', while in summer the soil is receiving *more* moisture compared to the CTRL-run. Hence, from fall to spring, the increase in net water influx ($P-E$) was lower then the increased runoff, i.e. $\Delta(P-E) < \Delta RO$. While in summer, $\Delta(P-E) > \Delta RO$. This is in accordance with a more frequent cessation of evaporation due to soil dessication below the wilting point (if suddenly $E=0$, $P-E$ will increase).

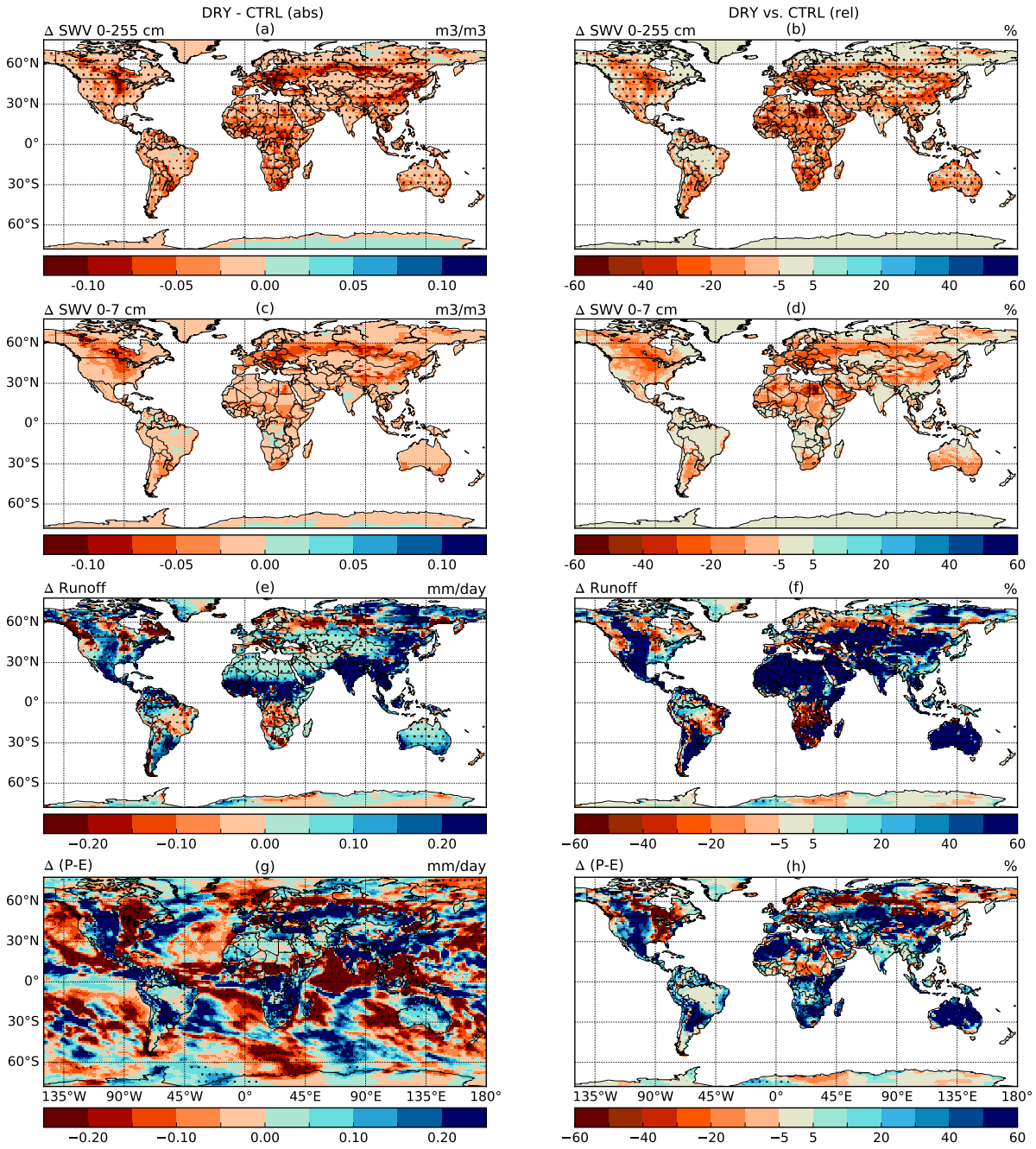

Figure 26: Adjustment of the soil hydrology (JJA mean). The first columns represent the absolute difference (DRY - CTRL) in mm/day and the second column the relative change (in %) with respect to the CTRL run. (a, b) Weighted vertical integral over the 4 land surface model levels (0-255cm) of the soil water volume (θ). (c, d) Soil water volume of top layer. (e, f) runoff. (g, i) precipitation - evaporation, i.e. the net hydrological exchange with the atmosphere.

C.3 Atmospheric Hydrology (summer)

The decrease in evaporation can trigger a multitude of responses (i.e. decrease in the water content, affecting boundary layer stability, increase in moisture convergence due to dynamics or due to an increased moisture gradient). The evaporation-precipitation interacted, and the result is that precipitation also decreased substantially, see figure 27(c, d). To further illustrate the evaporation-precipitation interaction, a contour-line of the precipitation change (black for positive, blue for negative) is drawn over the evaporation change, both in figure 27(a, b) and 27(c, b). The contour-line clarifies that in summer, on the Eurasian continent, the pattern of the adjusted precipitation and evaporation closely overlap. Precipitation changes mediated through large scale dynamics are not restricted to the regional perturbation. The fact that evaporation and precipitation change closely overlap hints at the dominance of their local interaction (and not changes in precipitation driven by adjusted large scale circulation).

From another perspective, the contour-line also show that the latter mentioned precipitation change is occurring quasi-local of the evaporation change, thereby referring to the precipitation decrease occurring adjacent to the location of the evaporation decrease. This generally occurs downwind of the evaporation change, see Northern Eurasia at 60°N and Eastern North American at 0°W. The observed downwind decrease in precipitation (over regions initially untouched by the perturbation) appears to be associated with a decrease in moisture convergence (Fig. 27e, but the decrease in moisture (≈ -0.25 mm/day) appears insufficient to explain the total decrease in precipitation (≈ -0.5 mm/day). As can be read in section **??**, the complete hydrological response can only be explained when encompassing the energetic response (change in incoming radiation, energy partitioning and atmospheric stability).

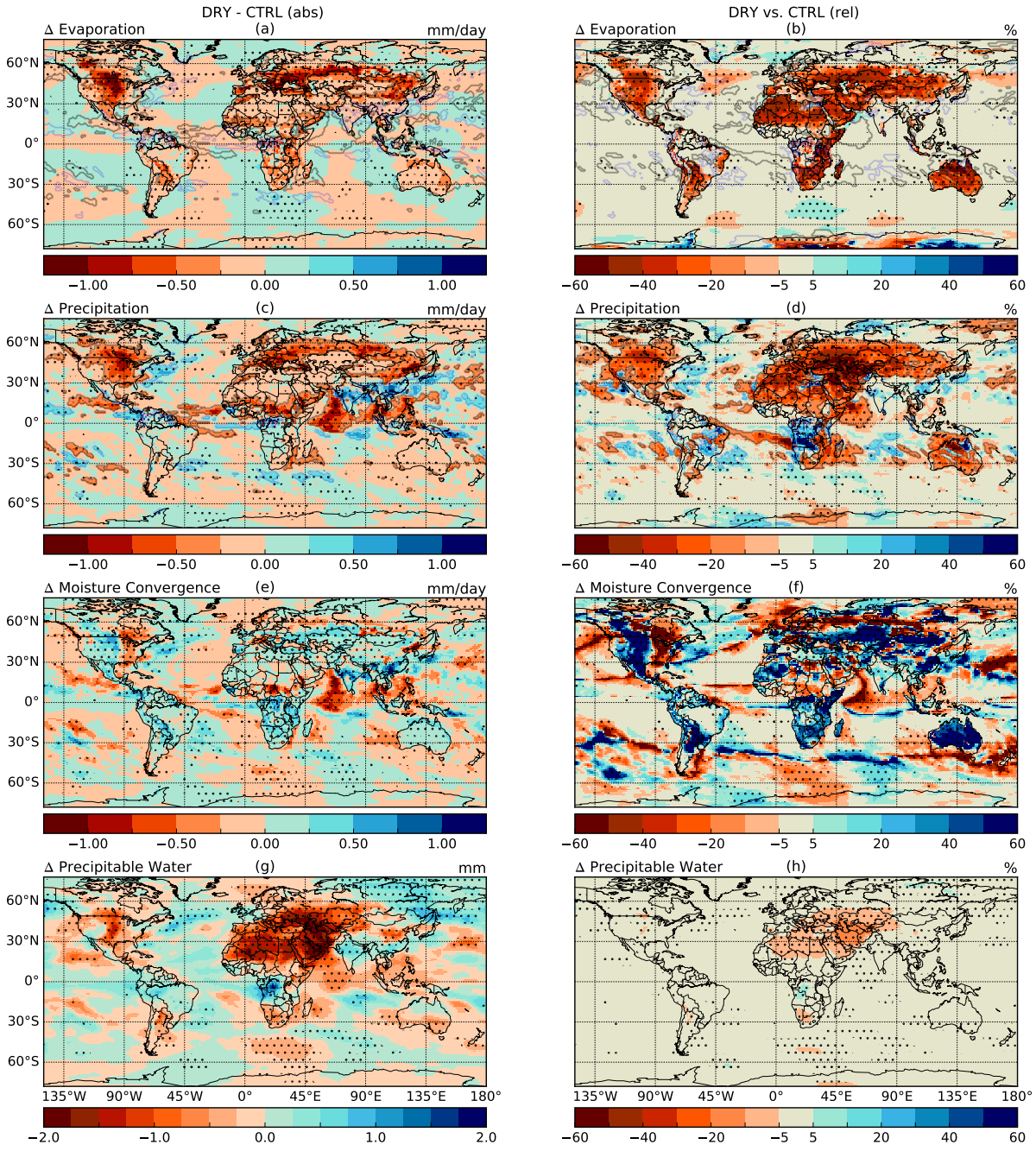

Figure 27: Change in atmospheric hydrology in summer (JJA). Plots show the change in climatological mean of (a, b) evaporation, (c, d) precipitation, (e, f) moisture convergence and (g, h) precipitable water. A black (blue) contour line is drawn in case of a positive (negative) precipitation change in 27(a, b) and 27(c, b). The contour lines are drawn at (+/-)0.05 mm/day and (+/-)10%.

C.4 Energetic Response (summer)

The hydrology and energetics are interlinked in multiple ways. In our experiment, the surface air temperature can be affected by a change in; net absorbed surface shortwave radiation (ΔR_{net}), the partitioning of R_{net} (into sensible, latent and ground heat flux) and a change in circulation (advection of warmer/colder air).

The decrease in evaporation alters the partitioning of R_{net} (figure 28). This means an increase of radiative energy used for heating the soil, thereby increasing the ground and sensible heat flux. In return, an increase in the soil temperature will benefit evaporation, providing a negative feedback (top layer/skin temperature is implicitly taken into account when calculating the evaporative flux in the land surface model (ECMWF, 2011)). Moreover, the increase in surface temperature decreases the relative humidity, hence, increases the Conversely, increased surface temperature are associated with more stagnant weather formation (Zampieri et al., 2009). Although the decrease in atmospheric static stability ($\frac{\delta T}{\delta z}$ increases) will favor dry convection.

The decrease in precipitable water can affect clouds. The amount of surface shortwave downward radiation is used as a proxy for the change in cloud cover (figure 29a, b). The dry (Hadley subsidence) regions render the greatest decrease in precipitable water (figure 27g), yet there were already hardly clouds present in the CTRL. Hence, it does not have a large impact on the surface solar radiation. Around the peripheries of the perturbation, however, a significant decrease in cloud cover is observed. Indicating that the decrease in triggered precipitation occurs in concert with a decrease in the generation of clouds. This feature is rendering a positive feedback between cloud cover (surface shortwave downward radiation) and desiccation.

The surface air temperature renders a significant response (regionally around +3°C, +15%), see figure 29. The summer response appears to closely match the northern hemisphere absolute change in radiative partitioning and the change in net surface shortwave radiation. The air at 500 hpa also rendered a significant increase (figure 29e). Interestingly, one could argue that a decrease in clouds is associated with a decrease in latent heat release up in the atmosphere, thereby cooling the upper tropospheric air. Apparently, the increase in turbulent and sensible heat flux are dominant components that are heating the upper air.

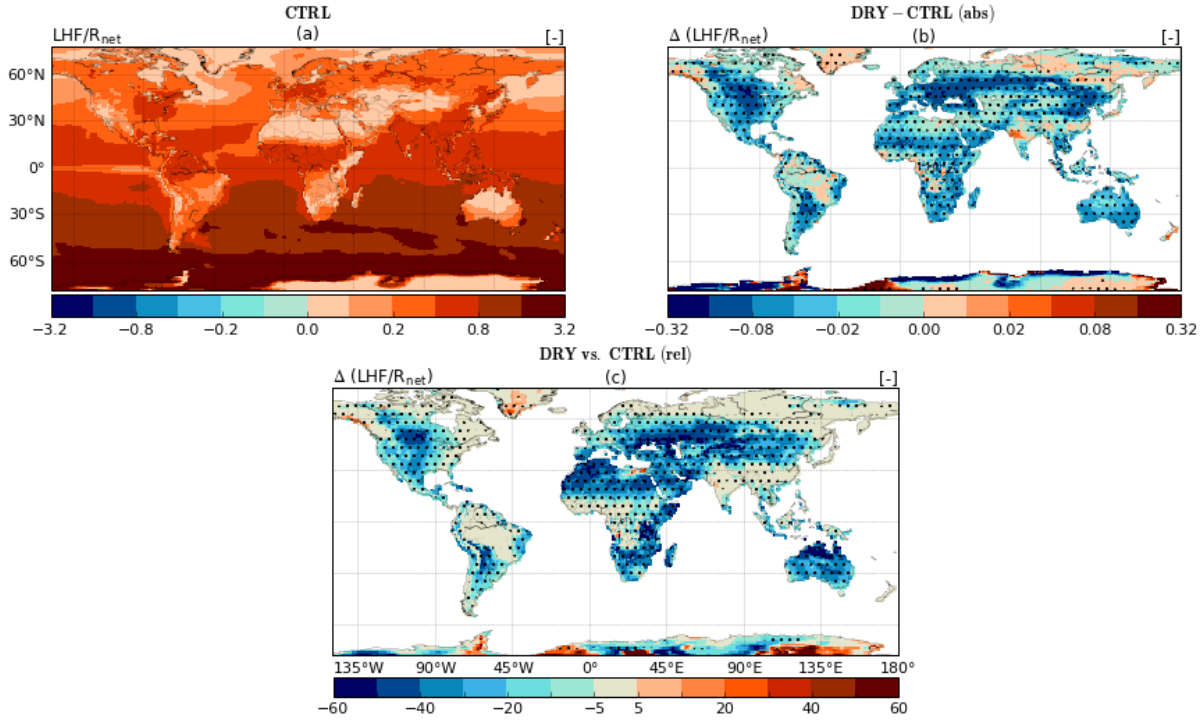

Figure 28: Plot (a) shows the portion of radiative energy going into the latent heat flux. Plots (b) and (c) show the change in the amount of net surface radiation going into the latent heat flux in absolute and relative terms.

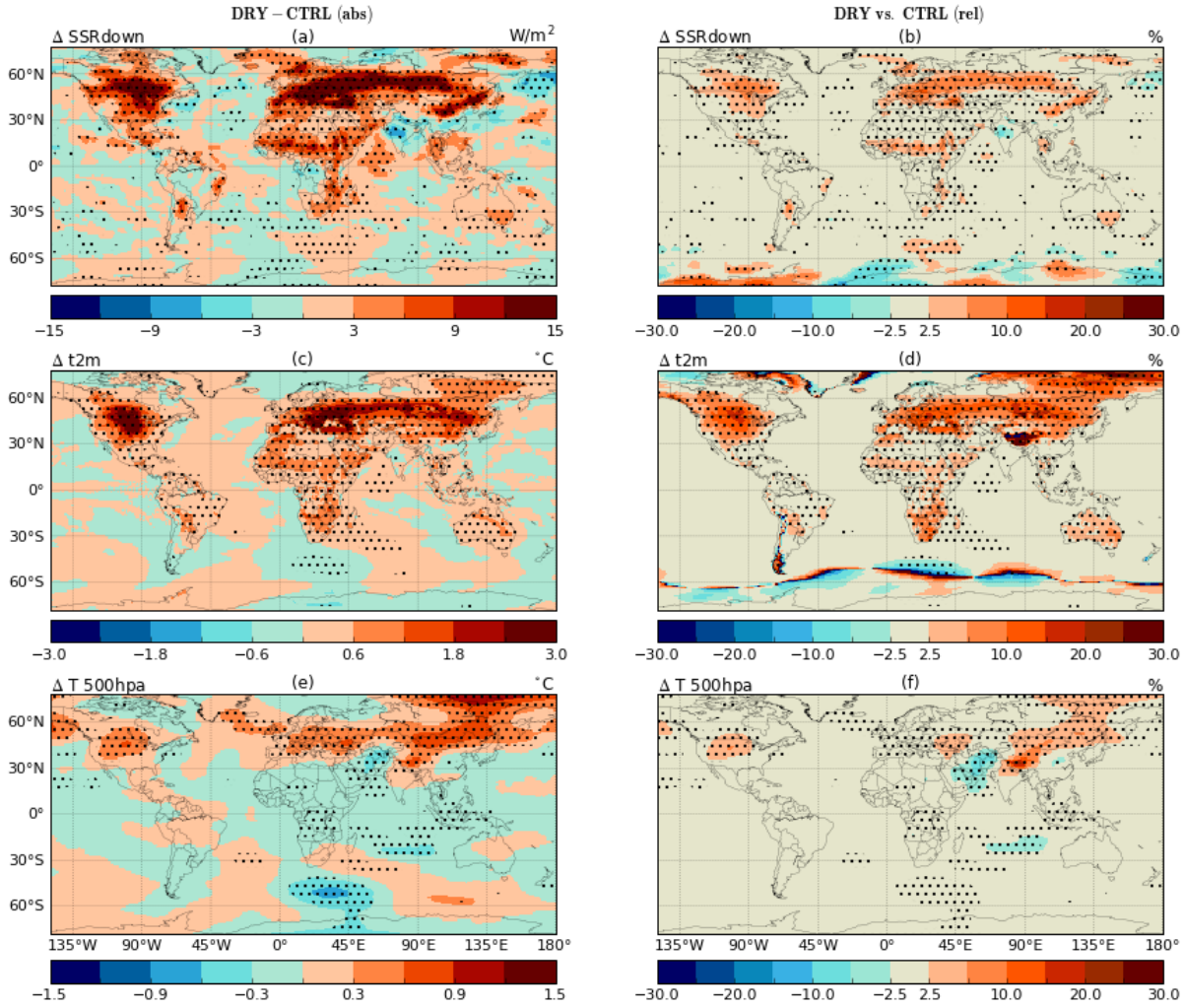

Figure 29: Plot (a) and (b) show the change in surface shortwave radiation downward in absolute and relative terms, which is also a proxy for the change in cloud cover. The change in the surface temperature in shown in plot (c) and (d). The change in the temperature at 500 hpa is shown in plot (e) and (f).

D Model response to SRO perturbation in spring

To elucidate the experiment further, it is insightful to further discuss the response in spring - when soils are generally still wet from winter. We present the figures in the same order as done above and subsequently discuss the differences.

The perturbation (RO/P) in spring is a bit stronger and spatially similar to what occurs in summer (see figure 30). As was stated earlier, the dessication of the entire soil column is quite constant throughout the year. In spring, the top layer dessicated substantially less (see figure 31). The response in runoff is relatively similar, but the response of the soil net water influx ($P - E$) (see figure 31g) is substantially less compared to what we observed in summer, see figure 26g.

The response in the atmospheric hydrology is also meager compared to summer (see figure 32). The absolute change in evaporation is low, although relatively it becomes substantial. The (relative) change usually follows the top layer desiccation better and hence, also matches the impact of the increased runoff-efficiency much better compared to summer. Therefore, the dessication in spring (winter and fall) appears to be a direct effect of our perturbation. With a low change in evaporation, the evaporation-precipitation interaction generally cannot arise in a consequential manner, hence, precipitation hardly changes over land.

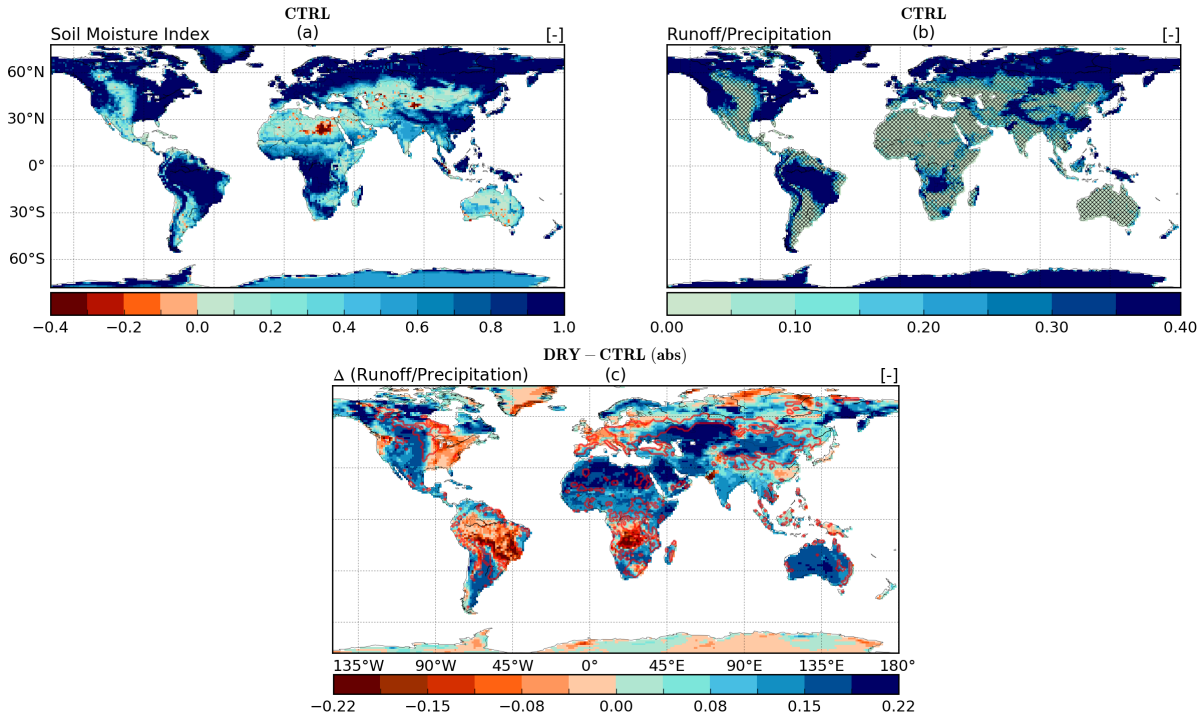

Figure 30: Visualizing the perturbation in spring, as done in figure 25.

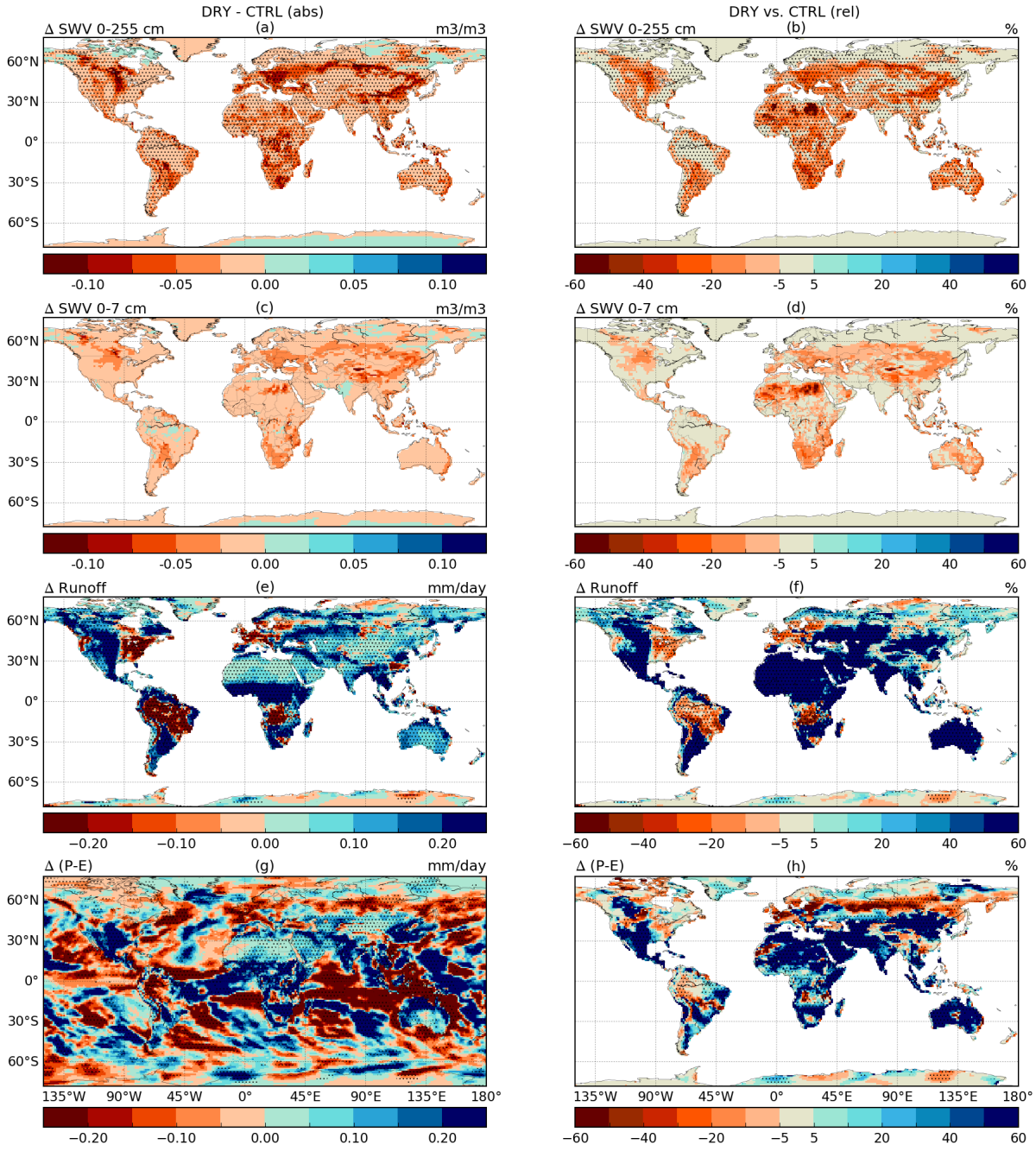

Figure 31: Adjustment of the soil hydrology in spring (MAM). See caption of figure 26.

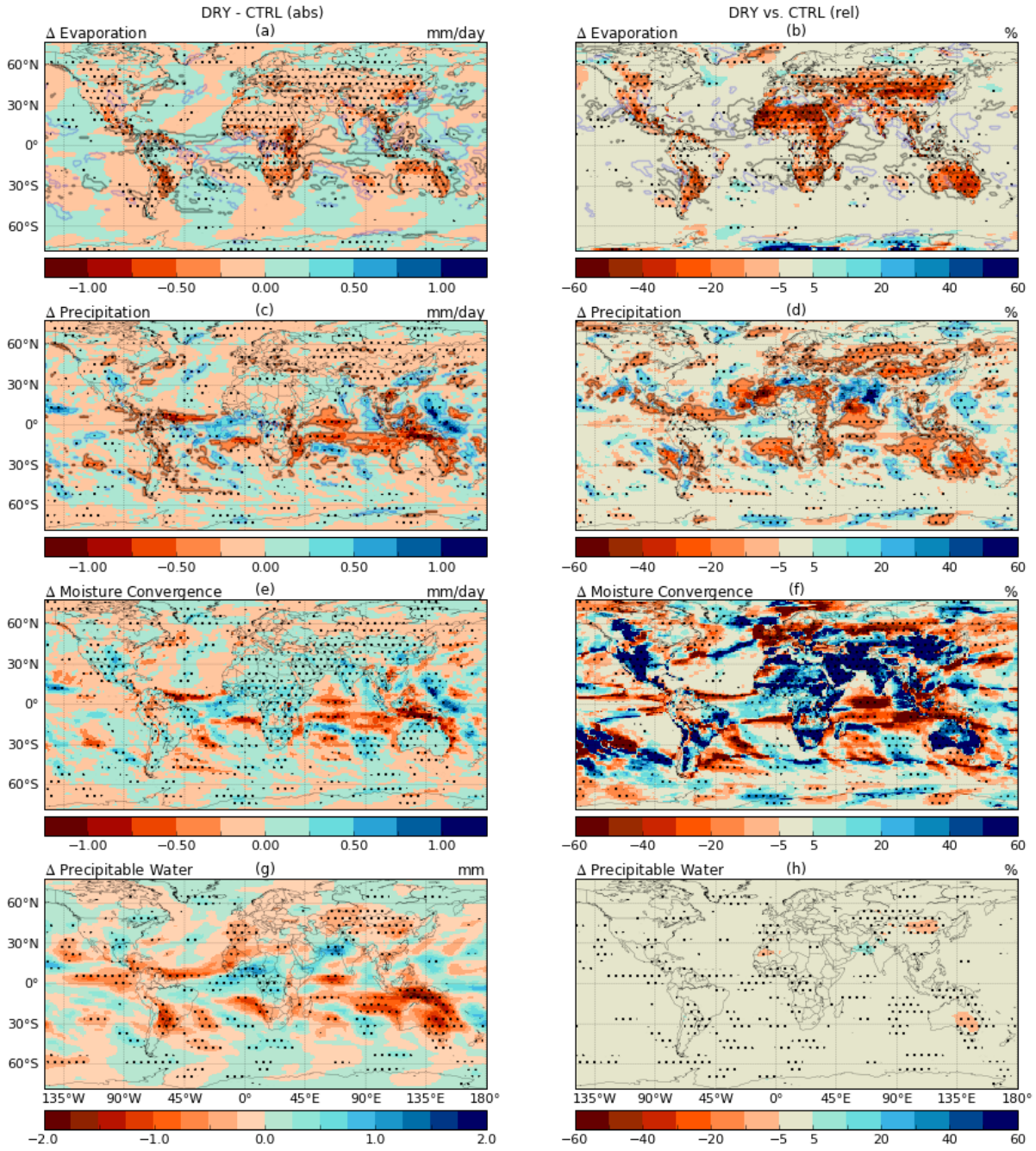

Figure 32: Change in atmospheric hydrology in spring (MAM). See caption of figure 27

E Land-Precipitation coupling metric

We first analyze the land-precipitation coupling globally for the CTRL (EC-earth) in summer and winter (Fig. 14a and **??**a). We again observe that the land-precipitation coupling is strongest (most positive) in the summer hemisphere. It appears especially strong approaching the Arctic region. Unfortunately, due to technical details of the tracking model, the algorithm becomes decreasingly reliable approaching the poles (model tracks between 78°S and 78°N).

We can distinguish the northern hemispheric warm ocean currents (i.e. gulf stream and North Pacific Current). Above these warm water masses, we know there is increased precipitation compared to its surroundings (not shown). It is therefore intuitive to think that this increased precipitation is related to the local high oceanic evaporation. Hence, ζ conveys that, indeed, precipitation is more often occurring in concert with above average q_o/q. The metric also shows where this effect is advected land inwards. Around the Caspian and Black sea, we observe the same effect of oceanic evaporation on the precipitation events. The warm oceanic currents on the southern hemisphere are not similarly visible, possibly because the impact of the southern currents on precipitation is much less pronounced (not shown).

Similarly, in the winter hemispheres, we expect a higher oceanic-precipitation coupling at the coastlines (negative ζ). Since, oceanic evaporation is strongest in winter while land evaporation is weakest. This feature is generally visible on most continental coasts, with the strongest exception for southern-America (in southern-America the continental evaporation remains to be important for precipitation). Possibly due to the large amount of continental evaporation by the Amazonian forest. Over the Inter Tropical Convergence zone, we expect that the oceanic water content (q_o/q) is high, but to be clear; the ratio will only change if precipitation is more often occurring with a certain preference in the water content. Hence, we do not expect a strong preference over the ocean. To conclude, over the oceans ζ is approximately zero ($P_c/P \approx q_c/q$), expect near coastlines or the golf streams. Land inwards, the land-precipitation coupling becomes (more) dominant in summer.

Hereafter, we analyzing the difference in land-precipitation coupling forced by our increased runoff experiment. Between Eurasia and Africa, we observe a strong spatial variability in $\Delta\zeta$. Possibly, this region renders a stronger variability due to the ocean-land arrangements (Mediterranean, Caspian and Black sea), which can interact (thermally and dynamically) more easily on a regional scale when responding to changes over the land surface. In the analysis of EC-earth versus ERA-Interim (section 3.3), these regions also render large differences, albeit not as spatially variable.

Relating large hydrological change in the northern hemisphere summer with the change in land-precipitation metric. It shows, to some extent, a weaker coupling at the peripheries of the perturbation (around 60°N), yet, it is not a very consistent signal. Excluding the ocean-land interactions at work around the Mediterranean and Arabic regions discussed earlier, the perturbed regions generally show an increased land-precipitation coupling.

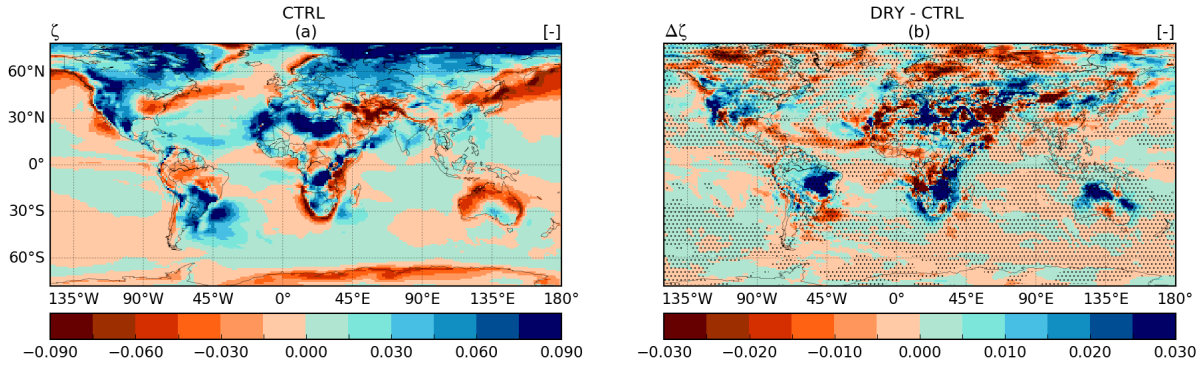

Figure 33: New metric representing the difference in continental recycling ratio independent of the background water composition (q_{tr}/q) for JJA.

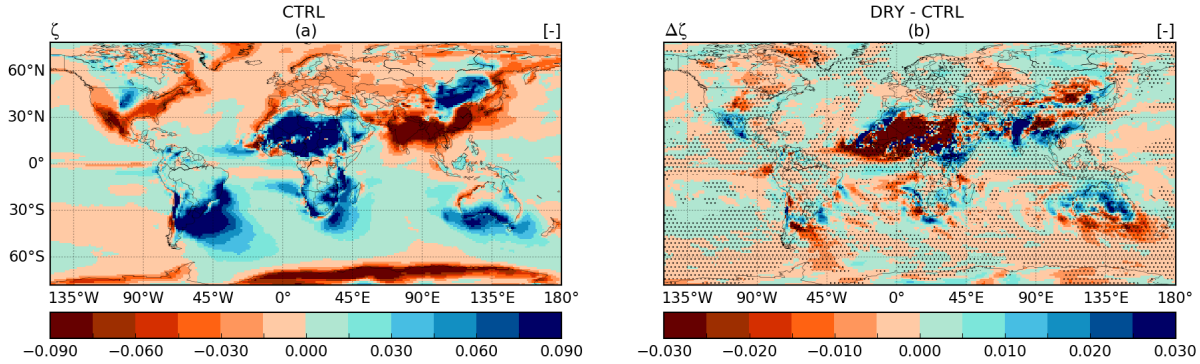

Figure 34: New metric representing the difference in continental recycling ratio independent of the background water composition (q_{tr}/q) for DJF.

F Sensitivity Desiccation to Source/Sink Perturbation

The fact that we observe moistening in the perturbed soils in summer (see Appendix **??**), induces a dampening effect on the annual mean desiccation. However, we remain to find it notable that the desiccation is substantially stronger at the peripheries compared to the perturbed regions. We wanted to address that another aspect of low desiccation in the perturbed regions is that the hydrological sensitivity of the soil desiccation (being between wilting point and field capacity) is more sensitive to a decrease in precipitation compared to an increase in runoff. This can be easily understood by the negative feedback that occurs when increasing the sink. Namely, the increase in sink, desiccates the soil, thereby decreasing the sink. Hence, the initial perturbation is dampened. When decreasing the source, this is not dampened.

To clarify the difference in drying response to a forcing, a simplified soil moisture-atmosphere feedback is presented schematically for both scenario's. In figure 35, we show the forcing due to a decrease in precipitation and in figure 36 we increase the runoff sink. We assume certain crude assumptions, but these assumption do not endanger the qualitative conclusion. For clarity, the feedback is discretized in time-steps of a day, whereas in truth, the two steps (e.g. step 2 and 3) subsequent to the perturbation, would occur simultaneous with the perturbation (step 1);

$\boldsymbol{P_i}$ $[\boldsymbol{t_0 \rightarrow t_1}]$ Initial Perturbation
The soil water mass balance is disrupted by a perturbation that will dry the soil by either increase the source (precipitation) or sink (runoff).

$\boldsymbol{A_S}$ $[\boldsymbol{t_1}]$ Adjustment Soil.
The soil receives $x\Delta$ mm less water, and hence this decrease is directly translated into a soil desiccation and associated decrease in sinks.
It is assumed the partitioning of $x\Delta$ mm between the two sinks remains constant. For example, if RO accounted for 20% of the source, then it will also decrease by 20% of $x\Delta$ mm.

$\boldsymbol{A_A}$ $[\boldsymbol{t_1}]$ Adjustment Atmosphere.
Positive evaporation-precipitation feedback renders a decrease in precipitation due to the decrease in evaporation, assuming $\Delta P = 0.5\Delta E$.

$\boldsymbol{P_r}$ $[\boldsymbol{t_1 \rightarrow t_2}]$ Response Perturbation.
The initial perturbation is maintained + the effect of the adapted soil water, sinks and precipitation.

$\boldsymbol{A_S}$ $[\boldsymbol{t_2}]$ Adjustment Soil.

$\boldsymbol{A_A}$ $[\boldsymbol{t_2}]$ Adjustment Atmosphere.

We cannot prove that this difference in sensitivity leads to substantial differences in dessication. Although we learned that the dessication in summer (forced by a decrease in precipitation), was substantial - especially considering the significant decrease in precipitation was only present in summer. While, the increased runoff was present in all seasons, the (relative) annual mean dessication of the top layer in perturbed regions is less (and over the entire column almost absent). However, the absence in the annual mean desiccation in dry regions can caused by the re-moistening during summer (since evaporation ceased in these regions).

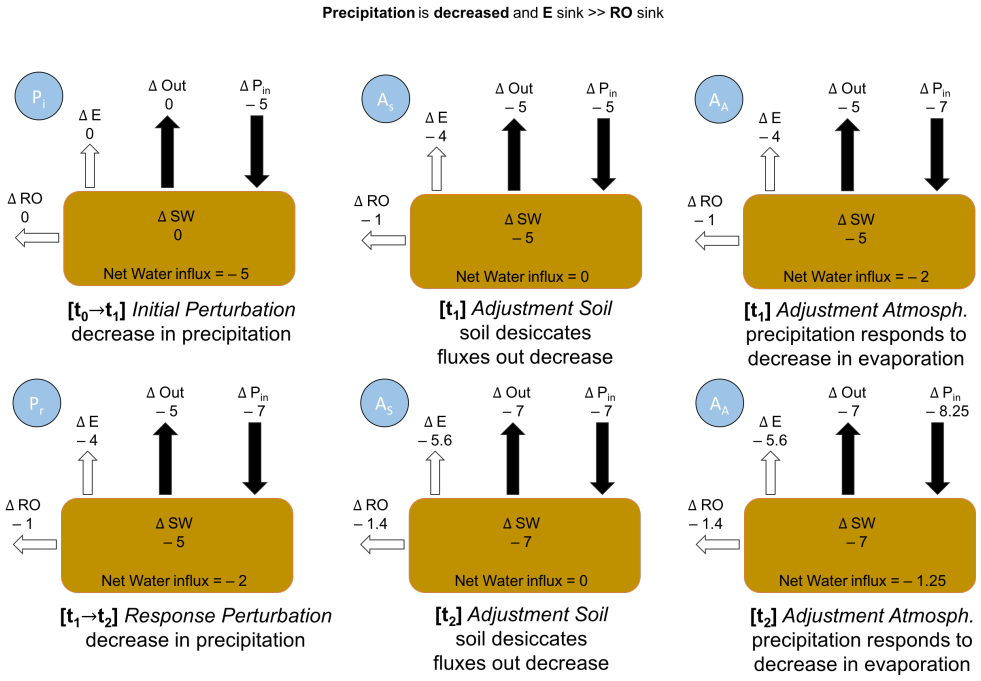

Figure 35: The dessication is forced by a decrease in source (precipitation). For further explanation and assumption, see enumeration above. We assume that evaporation is the dominant sink (removing 80% of P), while RO is minor (removing 20% of P). ΔOut is the cumulative sink, the net water influx $= \Delta P_{in} + \Delta Out$.

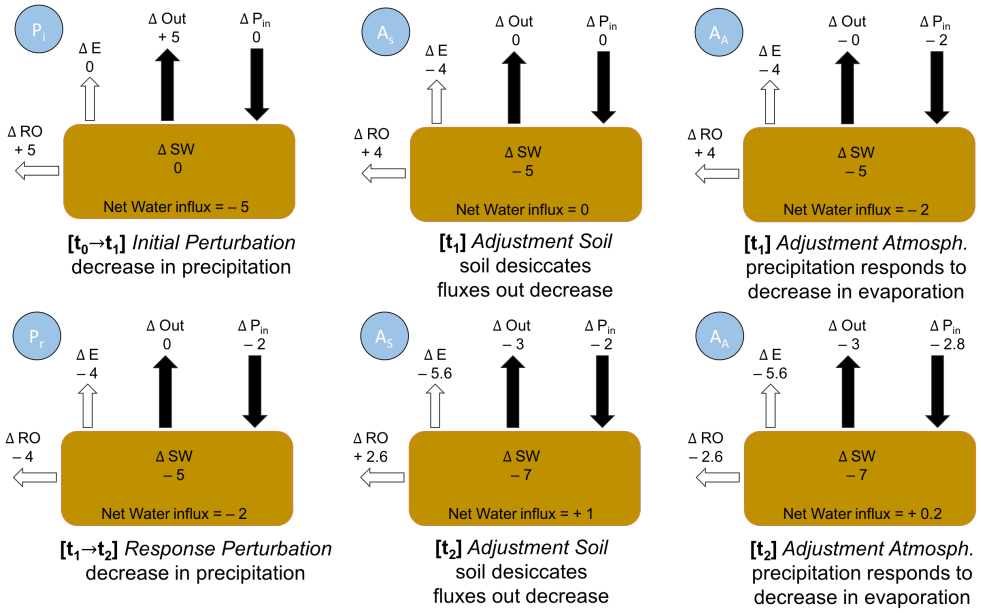

Figure 36: Same as figure 35, yet now we attempt to dessicate the soil by increasing the runoff sink.

In 36, we observe that the increased RO-sink is dampened by the decrease in the evaporative sink. Note, that in step 2 the net water influx has become positive since the $\Delta Out < \Delta P_{in}$. In figure 35, the net water influx remains negative, i.e. further drying the soil.